ALL ABOUT MAX: A MALE ADULT VOXEL PHANTOM FOR MONTE CARLO CALCULATIONS IN THE AREA OF RADIATION PROTECTION DOSIMETRY

R Kramer [1], J W Vieira [1], H J Khoury [1] , F R A Lima [2] and D Fuelle [3]

[1] Departamento de Energia Nuclear, Universidade Federal de Pernambuco, Av. Prof. Luiz Freire, 1000, Cidade Universitária, CEP: 50740-540, Recife, PE, Brazil

[2] Centro Regional de Ciências Nucleares, Rua Cônego Barata, 999, CEP: 52110-120, Recife, PE, Brazil

[3] Eschenstrasse 68, 85716 Unterschleissheim, Germany

E-mail: rkramer@uol.com.br

Statement of provenance:
'This is an author-created, un-copyedited version of an article accepted for publication in Physics in Medicine and Biology. IOP Publishing Ltd is not responsible for any errors or omissions in this version of the manuscript or any version derived from it. The definitive publisher authenticated version is available Online at stacks.iop.org/PMB/48/1239. '

Abstract. The Male Adult voXel (MAX) phantom has been developed from an already existing human voxel model, in order to arrive at a representation of the human body as close as possible to the anatomical specifications of the ICRP Reference Adult Male. MAX can be used in the area of computational dosimetry with regard to internal and external exposures of the human body to ionizing radiation, as to determine equivalent dose to organs and tissues for the purposes of radiation protection. After a review of recent human phantom dosimetry, this paper describes the construction of the MAX phantom with respect to the masses of the soft-tissue organs, the design of a the special dosimetric model applied to the skeletal tissues, and the creation of a computational exposure model made of the MAX phantom and the EGS4 Monte Carlo code. Conversion coefficients between equivalent dose to the red bone marrow as well as effective dose and air-kerma free in air for external photon irradiation from the front and from the back, respectively, are presented and compared with similar data from other human phantoms. From this comparison it can be concluded that the MAX/EGS4 exposure model is suitable for equivalent dose calculation in the area of radiation protection

1. Introduction

The basic dosimetric quantity related to the probability of appearance of stochastic radiation effects as defined by the International Commission on Radiological Protection (ICRP) is the effective dose, which "is the sum of the weighted equivalent doses in all tissues and organs of the body. It is given by the expression

$$E = \sum_T w_T H_T$$

where H_T is the equivalent dose in tissue or organ T and w_T is the weighting factor for tissue T" (ICRP 1991). The Commission recommends weighting factors for 12 tissues and organs, plus for a so-called "remainder", which is composed of another 10 organs and tissues (table 1). The trachea replaced the upper large intestine (ICRP 1994), which earlier was part of the remainder (ICRP 1991), but actually is already included in the colon from the main list. H_T represents the equivalent dose averaged over the volume of tissue T, which reflects the assumption of a linear dose-risk relationship.

Table 1. Tissue weighting factors as defined by ICRP60

Tissue/organ	Tiss.weight.f.
	w_T
Gonads	0.20
Red bone m.	0.12
Colon	0.12
Lung	0.12
Stomach	0.12
Bladder	0.05
Breast	0.05
Liver	0.05
Oesophagus	0.05
Thyroid	0.05
Skin	0.01
Bone surface	0.01
Remainder	0.05

Remainder organs: Adrenals, Brain, Trachea, Small Intestine, Kidneys, Muscle, Pancreas, Spleen, Thymus and Uterus

Effective dose is the most important quantity of the protection philosophy of ICRP60 (ICRP 1991), and as a consequence dose limits for stochastic effects recommended by the Commission are expressed in terms of effective dose. Therefore it becomes the main task of radiation protection dosimetry to determine equivalent dose to the 22 organs and tissues at risk as defined by the ICRP.

Matter, after having been exposed to ionizing radiation, cannot express itself in terms of absorbed dose or equivalent dose. Consequently equivalent dose in tissues of the human body cannot be measured directly. Indirect measurements of equivalent dose can be made by the use of radiation detectors, but they are practically restricted to locations on the surface of the human body, thereby excluding most of the 22 organs and tissues from this method of equivalent dose assessment.

In order to establish relationships between protection quantities to be determined and operational quantities which can be measured one has to make use of an exposure model. An exposure model is a physical and/or computational arrangement for the simultaneous determination of equivalent dose in the human body and of measurable quantities for exposure conditions relevant in radiation protection. It must therefore incorporate sources and fields of the radiations involved a model of the human body, a method for the determination of equivalent dose inside the human body, and a possibility to determine measurable quantities of interest. The results are usually expressed as conversion coefficients (CCs), which are ratios between equivalent dose to organs and tissues at risk and measurable quantities. Routine measurements in radiation protection can easily be interpreted in terms of effective dose by multiplying the instrument's reading with the corresponding CC, provided that the conditions simulated with the exposure model correspond to the real exposure situation.

For those involved in treatment planning for radiation therapy, CCs are a quite familiar concept. Percentage depth-dose, tissue-air ratios and backscatter factor are only some examples for ratios between a quantity of interest (absorbed dose at a point in human tissue) and a measurable quantity (kerma in air free in air, at the surface or inside a phantom, etc.). Exposure models for radiation therapy normally use homogeneous water phantoms with linear dimensions of about 30 cm (ICRU 1992). Absorbed dose distribution inside the phantom as well as the measurable quantity are either determined by measurement or by radiation transport calculation.

Radiation therapy CCs are too limited for the use in radiation protection with regard to almost all irradiation parameters, especially with respect to the field size, and cannot be applied to skeletal tissues, for example. But the CCs for treatment planning give valuable insight into the depth dose distribution in an extended body as function of radiation quality and field geometry, which even can be used in case

special CCs for radiation protection are not available, in order to avoid an equivalent dose estimate just by the detector reading of a free-in-air quantity.

Indeed, early physical exposure models for radiation protection using homogeneous phantoms have been modified therapy exposure models. Delafield (1963) measured depth-dose for a broad beam of photons and related the results to personnel dosimetry, while Spiers (1956) measured omni-directional gamma exposures to certain body tissues in a homogeneous water phantom and Spiers and Overton (1963) in a homogeneous wax phantom. A well-known heterogeneous physical model is the Alderson-Rando phantom (Alderson 1962), which consists of a human skeleton embedded in tissue-equivalent material which is molded to form the torso and head of a human body. The disk-like set-up of the phantom permits the positioning of small TLD dosimeters in a matrix of holes which have been drilled across each disk. Early measurements of various CCs with the Alderson-Rando phantom have been performed by A. R. Jones (1966).

Computational exposure models use radiation transport calculations based on solving the Boltzmann equation. Analytical methods are recommended especially for homogeneous and symmetrical media, while the statistical Monte Carlo Method lends itself for heterogeneous and geometrically complicated structures. Early CC calculations with semi-infinite homogeneous slabs mostly with 30 cm thickness have been done for neutrons by Snyder (1950) and Alsmiller et al (1970), and for electrons and photons by Snyder (1965), Alsmiller and Moran (1968), Beck (1970), Berger and Seltzer (1969), and Irving et al (1967). Soon the semi-infinite slab was replaced by an elliptical cylinder (Auxier et al 1969, Sidewell et al 1969, Snyder 1971), in which Sidwell and Burlin (1973) introduced inhomogeneities, like lungs. Numerous of these measured and calculated CCs have been published by the ICRP in Publication No.21 (ICRP 1973).

With respect to the determination of CCs for the 22 different organs and tissues specified by the ICRP, the development of mathematical heterogeneous human phantoms was a major breakthrough. In mathematical human phantoms size and form of the body and its organs are described by mathematical expressions representing combinations and intersections of planes, circular and elliptical cylinders, spheres, cones, torii, etc.

Fisher and Snyder (1967, 1968) introduced this type of phantom for an adult male which also contains ovaries and a uterus. During the compilation of the Report of the Task Group on Reference Man, Publication No.23 (ICRP 1975) the phantom has been further developed by Snyder et al (1974a, 1978). Since then it is known as “MIRD-5 phantom” (Medical Internal Radiation Dose Committee (MIRD) Pamphlet No.5).

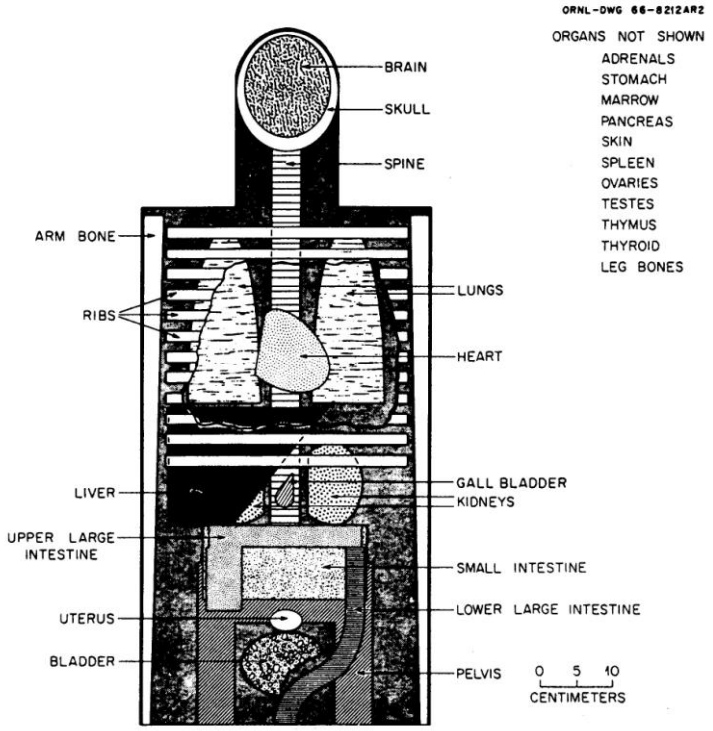

Figure 1. Coronal view of the mathematical MIRD-5 phantom. From Cristy and Eckerman (1987

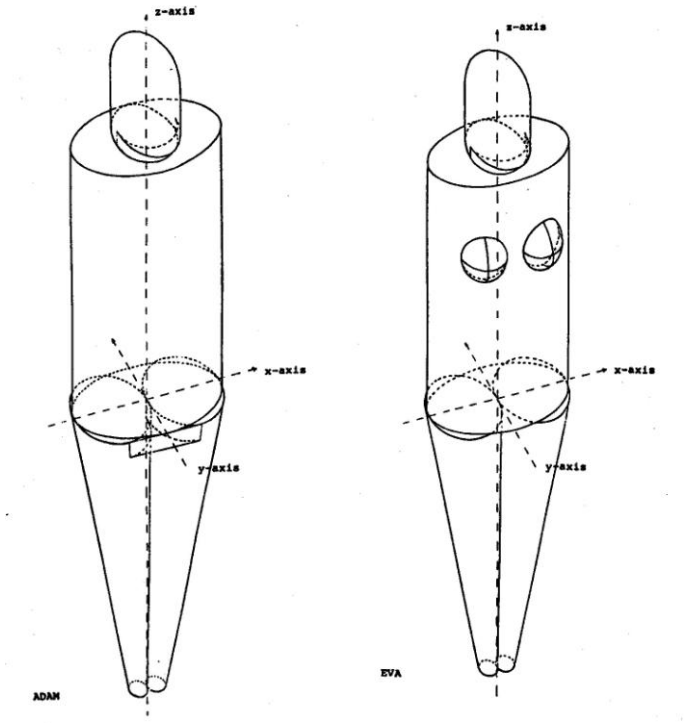

Figure 2. The mathematical ADAM and EVA phantoms. From Kramer et al (1982a)

The MIRD-5 phantom (figure 1) has been the basis for various derivations representing infants and children of various ages (Cristy1980), gender-specific adult phantoms (Kramer et al 1982a) (figure 2) and a pregnant female adult phantom (Stabin et al 1995). Body height and weight as well as the organ masses of these MIRD-type phantoms are in accordance with the Reference Man data (ICRP1975). Connected with the ALGAM Monte Carlo code (Warner and Craig 1968) the MIRD-type phantoms represent computational exposure models which permit the determination of CCs for all 22 organs and tissues considered at risk by ICRP. For photon irradiation CCs have been calculated with the original MIRD model by Snyder and co-workers from the Oak Ridge National Laboratory USA mainly for internal exposures (Snyder 1974b, 1975, Cristy and Eckerman 1987), while Kramer and co-workers from the GSF Research Center, Germany used the "MIRD-5-modified" gender-specific ADAM and EVA phantoms to calculate external exposures (Drexler and Kramer 1977, Kramer and Drexler 1979b, Kramer and Drexler 1982b, Zankl et al 1997). Many CCs for external and internal exposures have been published by the ICRP (ICRP 1979, 1987, 1996) and also by the International Commission on Radiation Units (ICRU 1998), which has published also a special report on phantoms (ICRU 1992).

For the present, tomographic or voxel phantoms represent the latest step in the improvement of exposure models. Tomographic phantoms are based on digital images recorded from scanning of real persons by computed tomography (CT) or magnetic resonance imaging (MRI). Each image consists of a matrix of pixels (picture elements), which number depends on the resolution chosen during scanning. A consecutive set of such images can be considered as a three-dimensional matrix made of voxels (volume pixels), where each voxel belongs to a specific organ or tissue. Compared to the mathematical phantoms, voxel phantoms are true to nature representations of the human body, and their voxel structure allows to determine distributions of dose even within an organ or tissue, which could become important in case of radiation accidents.

Tomographic or voxel phantoms have been introduced by Gibbs et al (1984) and independently also by Williams et al (1986), who extended this effort to construct infant and children voxel phantoms (Veit et al 1989) as well as a "voxelized" version of the Alderson-Rando phantom (Veit et al 1992). Meanwhile these activities have produced a whole family of voxel phantoms (Zankl and Wittmann 2001, Petoussi-Henss et al 2002).

Zubal et al (1994a, 1994b, 1995) segmented CT and MRI data of a patient who was scanned from head to mid-thigh. Dimbylow (1995a) introduced the voxel phantom NORMAN based on MRI data of a healthy volunteer. The voxel dimensions have been scaled to match body height and weight of the Reference Man (ICRP 1975), that is a body weight of 70kg and a body height of 170cm.

Caon et al (1997) developed a voxel phantom of a 14 year old girl, Saito et al (2001) segmented whole-body CT data of a patient whose external dimensions were in good agreement with the Japanese Reference Man (Tanaka et al 1989), and Xu et al (2000) segmented color photographs of the Visible Human Male (Spitzer and Whitlock 1998) for the construction of the VIPMAN voxel phantom.

Many references on voxel phantoms can be found in the proceedings of an international workshop on voxel phantom development (Dimbylow 1995b) and in the publication of the GSF voxel family (Petoussi-Henss et al 2002).

For external exposures voxel CCs have been calculated for CT examinations by Zankl et al (1993) for the pediatric BABY and CHILD voxel phantoms, by Caon et al (1997, 1999) for a 14-year-old female torso voxel phantom, and Jones (1997) determined organ equivalent dose in the NORMAN voxel phantom arising from external photon irradiation. Segmented images from Zubal et al (1994a, 1994b, 1995) have been used by Ligot et al (1998) to perform a follow-up dosimetry for patients who underwent radiotherapy for skin haemangioma in childhood. Chest and lumbar spine examinations have been simulated by Zankl et al (2000) with the adult male voxel phantom GOLEM to study the influence of phantom diameter on patient dose. Equivalent dose to air-kerma CCs have been determined by Saito et al (2001) for the OTOKO voxel phantom and by Chao et al (2001a) for the VIPMAN voxel phantom for external exposure to photons, and also by Chao et al (2001b) for the same phantom for external exposure to electrons. In most of the cited studies air-kerma free in air or at the phantom's surface was the normalization quantity for the CCs.

For internal exposures Petoussi-Henss and Zankl (1998) published photon specific absorbed fractions for the pediatric BABY and CHILD voxel phantoms as well as for the adult voxel phantoms GOLEM and VOXELMAN (Zubal et al 1994a). These studies have been continued by Smith et al (2000,2001) and the data have been compared to those of the MIRD-5 system. Voxel data from Zubal et al (1994a,1994b,1995) have been used by Johnson et al (2000) to determine CCs for organ equivalent dose normalized to activity and by Yoriyaz et al (2000) and by Stabin and Yoriyaz (2002) to calculate specific absorbed fractions to be used in nuclear medicine.

2. The MAX phantom: Soft-tissue organ masses

2.1. Data base: The YALE VOXTISS8 voxel phantom

Acquisition of an appropriate set of images and the laborious process of segmenting many organs and tissues in an anatomically correct manner are the two main suppositions for the construction of tomographic or voxel phantoms, which sometimes are difficult to find and/or to realize, respectively. Fortunately the results of the voxel phantom development by Zubal et al (1994a, 1994b, 1995) have been made accessible for the scientific community on a website of the YALE university (Zubal 2001), thereby making the construction of the MAX phantom possible.

Three segmented voxel phantoms are among the data, which are available on the website of the YALE University:

- VOXELMAN: A torso voxel phantom with head,
- MANTISSUE3-6: The VOXELMAN phantom with legs and with arms, which are closed in front of the abdomen, and
- VOXTISS8: The MANTISSUE3-6 voxel phantom with the arms straightened along the sides of the body.

All three phantoms have been constructed with the same data base, namely 78 CT images acquired from neck to midthigh with 1-cm slice thickness, 51 CT images of the head and neck region with 0.5-cm slice thickness, and 124 high-resolution transverse MRI images with 0.15-cm slice thickness from a patient, who was scheduled for head, thorax, abdomen and pelvic scans for diagnosis of diffuse melanoma. His height was 175 cm and the weight was 70.2 kg.

VOXELMAN represents the combination of the segmented head and body CT images with a 4mm cubic voxel size. Later arms and legs, segmented form the Visible Man's red color cross-sections (Spitzer

and Whitlock 1998), have been added by M.Stuchly (1996) to the torso phantom, which then has been called MANTISSUE3-6. This phantom has been resampled to achieve a 3.6mm cubic voxel size.

Finally the arms of the MANTISSUE3-6 phantom have been straightened along the sides of the body by K. Sjogreen (1998), maintaining the 3.6mm cubic voxels. This version has been called VOXTISS8, and it consists of 487 segmented body cross-sections, each of which expands into a 192 x 96 pixel matrix. About 40 organs and tissues have been segmented in the trunk, arms and legs, and about 56 organs and tissues in the head. The VOXTISS8 phantom contains the high resolution MRI head, and it was this voxel model which has been chosen as data base for the construction of the MAX phantom.

A voxel model of the human body is a 3-dimensional matrix of small geometrical units (voxels), to which, depending on their location, organ identification number have been assigned. The media identification number and the associated material, which is to fill a voxel, have still to be defined by the user. Tissue compositions and densities, as well as mixtures of these materials, used in this study are taken from or are based on the ICRU Report No.44 (ICRU 1989), and are shown in table 2. The composition and density of soft tissue has been averaged from the data for brain, colon, heart, kidneys, liver, pancreas, spleen, testes and thyroid.

Table 2. The MAX phantom: Tissue compositions and densities based on ICRU44

Atomic No.	1	6	7	8	11	12	15	16	17	19	20	26	53	Density
Symbol	H	C	N	O	Na	Mg	P	S	Cl	K	Ca	Fe	I	
	[%]	[%]	[%]	[%]	[%]	[%]	[%]	[%]	[%]	[%]	[%]	[%]	[%]	[g/cm**3]
SOFT TISS	10,5	12,5	2,6	73,5	0,2		0,2	0,18	0,22	0,21	0,01	0,01	0,01	1,05
ADIPOSE	11,4	59,8	0,7	27,8	0,1			0,1	0,1					0,95
LUNG	10,3	10,5	3,1	74,9	0,2		0,2	0,3	0,3	0,2				0,26
MUSCLE	10,2	14,3	3,4	71	0,1		0,2	0,3	0,1	0,4				1,05
SKIN	10	20,4	4,2	64,5	0,2		0,1	0,2	0,3	0,1				1,09
CARTILAGE	9,6	9,9	2,2	74,4	0,5		2,2	0,9	0,3					1,1
BONE	3,4	15,5	4,2	43,5	0,1	0,2	10,3	0,3			22,5			1,92
RED BM	10,5	41,4	3,4	43,9			0,1	0,2	0,2	0,2		0,1		1,03
YELL BM	11,5	64,4	0,7	23,1	0,1			0,1	0,1					0,98

BM: Bone Marrow

Table 3 lists the body organs and tissues, most of which are relevant to radiation protection, together with their masses from ICRP23 (ICRP1975) and ICRP70 (1995) and for the VOXTISS8 phantom, respectively. For this investigation the revised body weight of 73 kg and body height of 176 cm, respectively, have been adopted (ICRP 1994, 1995)

Table 3. Organ and tissue masses for the ICRP Reference Male and the VOXTISS8 phantom

	ICRP 23/70	YALE	Perc. Diff.
ORG/TISS	Refer. Man	VOXTISS8	VOXT/Ref.M.
	[g]	[g]	[%]
Adipos. (Fat)	17200.0	14970.0	-13.0
Adrenals	14.0	3.0	-78.6
Bladder wall	45.0	154.2	+242.7
Skeleton	10500.0 *	13831.3**	(+31.7)
Brain	1400.0	1491.0	+6.4
Colon	725.0	895.7	+23.5
Eyes	15.0	15.8	+5.3
Kidneys	310.0	373.2	+20.4
Liver	1800.0	1434.0	-20.4
Lungs	1000.0	756.5	-24.4
Muscle	28000.0	36070.0	+28.8

Oesophagus	40.0	31.5	-21.3
Pancreas	100.0	38.8	-61.2
Red BM	1170.0	570.9	-51.2
Small Intest.	1040.0	1296.0	+24.6
Skin	2600.0	6676.0	+156.8
Spleen	180.0	272.8	+51.6
Stomach	400.0	251.5	-37.1
Testes	35.0	72.5	+107.1
Thymus	20.0	O	
Thyroid	20.0	5.1	-74.5
Trachea	10.0	14.3	+43.0
Total Body	73000.0	81730.0	+12.0
Height	176 cm	175.3cm	-0.4

Colon,Small Intestine and Stomach include contents
* Bone, marrow, cartilage, misc.
** Bone and marrow

The last column shows the percentage deviation of the VOXTISS8 organ masses relative to the ICRP data. As one can see the agreement between the two sets of data is poor. Only for the eyes and the brain the percentage difference is smaller than 10%. For all other organs and tissues the deviations are at least 20%, sometimes even higher than 100%.

In voxel phantoms the skin is usually represented by the first voxel layer at the body's surface. The high mass of the VOXTISS8 skin is due to the voxel thickness of 3.6 mm.

As for the higher weight of the VOXTISS8 phantom compared to the scanned patient, it has to be remembered, that arms and legs of VOXTISS8 came from the Visible Human (Spitzer and Whitlock 1998) who had a body weight of 104 kg and was 186 cm tall. But it is also obvious that the skeleton of the VOXTISS8 voxel phantom appears to be rather heavy for somebody who is 175.3 cm tall.

2.2. MAX: Changes and additions to organs

Table 4 shows the organ and tissue masses of the MAX phantom together with those for other computational models and the Reference Man data. The improvement with regard to the approximation to the Reference Man data can be seen in the last column which presents the percentage differences between the MAX phantom's organ and tissue masses and the ICRP Reference data.

In order to achieve this improvement, the volumes of the following VOXTISS8 organs have been:

- Increased: Adrenals, Liver, Lungs, Esophagus, Pancreas, Stomach, Thyroid, and
- Decreased: Bladder wall, Colon, Kidneys, Skin, Small Intestine, Spleen, Testes, respectively.

Apart from that, as only one adrenal was segmented in the VOXTISS8 phantom, therefore a second one had to be added.

The thymus and a part of the clavicles had not been segmented either. They have been added based on data found in ICRP23, ICRP70 and anatomical textbooks.

The thyroid has not only been enlarged, but also its position has been changed according to table 84 of ICRP23, where 2 cm of tissue overlying the thyroid are mentioned for the adult male. For frontal exposures this thickness is crucial, of course.

The volume of the trachea, already one of the smallest, has not been altered in order to permit a reasonable coefficient of variance in Monte Carlo calculations.

The volumes of the liver and the lungs could not be increased further to reach the Reference Man values without interfering with other organs. This is not considered to be problematic, because as these organs are already relatively voluminous, further moderate increase in volume would not change the average absorbed dose significantly.

Table 4. Organ and tissue masses for the ICRP Reference Male and various phantoms

	Math. Phant.	>>>>>>>> Adult human voxel phantoms <<<<<<<<<<					
	ICRP 23/70	GSF	GSF	NRPB	RPI	UFPE	Perc. Diff.
ORG/TISS	Refer. Man	ADAM	GOLEM	NORMAN	VIPMAN	MAX	MAX/Ref.M.
	[g]	[g]	[g]	[g]	[g]	[g]	[%]
Adipos. (Fat)	17200.0		19970.0	16513.0	36326.6	18350.0	+6.7
Adrenals	14.0	15.5	22.8	14.8	8.3	14.7	+5.0
Bladder wall	45.0	45.0	68.4	48.6	41.4	45.2	+0.4
Skeleton	10500.0	10175.0	10450.0	10177.0	11244.6	11146.5	+10.7
Brain	1400.0	1349.0	1218.0	1469.0	1574.0	1493.0	+6.2
Colon	725.0	724.0	534.0	732.0	2081.0	719.7	-0.7
Eyes	15.0		25.6			15.8	+5.3
Kidneys	310.0	284.0	316.0	318.0	335.4	307.5	-0.8
Liver	1800.0	1806.0	1592.0	1800.0	1937.9	1580.0	-12.2
Lungs	1000.0	1000.0	729.0	987.0	910.5	845.6	-15.4
Muscle	28000.0		26970.0	29177.0	43002.6	35880.0	+28.1
Oesophagus	40.0	39.7	30.1	42.1	38.9	39.6	-0.1
Pancreas	100.0	96.0	71.9	104.0	82.9	102.8	-2.8
Red BM	1170.0**	1500.0***	1177.0	1412.0	1128.6	1198.5	+2.4
Small Intest.	1040.0	1046.0	959.0	1081.0	1291.8	1032.0	-0.8
Skin	2600.0	3130.0	4703.0	4896.0	2253.4	3196.0	+22.9
Spleen	180.0	174.0	174.0	170.0	244.0	178.7	-0.7
Stomach	400.0	397.0	233.0*	292.0	497.7	397.0	-0.8
Testes	35.0	37.0	21.1	36.0	21.0 (1)	34.7	-0.9
Thymus	20.0	20.0	10.7	19.7	11.2	21.7	+8.5
Thyroid	20.0	20.0	25.8	20.0	27.6	19.8	-1.0
Trachea	10.0		13.7		7.3	14.3	+43.0
Total Body	73000.0	70450.0	68930.0	70000.0	104277.2	78256.9	+7.2
Height	176 cm	170cm	176cm	170cm	186cm	175.3cm	-0.4

Colon,Small Intestine and Stomach include contents
* Only Stomach wall
** ICRP 70
*** ICRP 23
(1) only one testicle
GSF = Research center for environment and health,Munich,Germany
NRPB = National Radiological Protection Board, Chilton, UK
RPI = Rensselear Polytechnic Institute, Troy, New York, USA
UFPE = Universidade Federal de Pernambuco, Recife, Brazil

The reduction of the skin volume has not been done by additional anatomical segmentation but rather by dosimetric separation. The user can choose any skin thickness below the 3.6mm voxel thickness. Depending on the location of the radiation interaction in the 3.6mm skin, the particle's energy loss will be deposited either in the new skin or in adipose tissue as a function of the thickness chosen. For the MAX phantom the skin thickness is 1.3 mm as defined by ICRP23.

The mass of the skeleton has decreased basically within the segmented volume given by the VOXTISS8 phantom. This has been achieved by a different distribution of the skeletal tissues, and will be explained in the 3. chapter.

Most of the organ masses are now in reasonable agreement with the Reference Man data. The remaining major deviations refer to the masses of the whole-body skin and the adipose and muscle tissues

of arms and legs. Apart from having already the ICRP23 skin thickness of 1.3 mm, with 3196g the total skin mass corresponds also already almost exactly to the new ICRP skin mass of 3220g of the upcoming revised version of Report No.23 (ICRP2001), and further reduction of the adipose and muscle tissues of arms and legs hardly would influence the absorbed dose to the critical organs in the trunk and the head.

Additions and modifications to all the soft-tissue organs together resulted in a net decrease of the total body weight by 787.3 g, while the re-distribution of the skeletal tissues reduced the total skeleton weight by another 2684.8 g. Consequently the MAX total body weight became 78256.9 g.

Figure 3 provides a coronal view through the MAX phantom. The cut is made in a depth where most of the spine is located. Figure 4 represents a cross-section through the body at a level where parts of the liver and the stomach can be seen, and figure 5 shows a cross-section through the MRI-head.

Figure 3. The MAX phantom: Coronal view

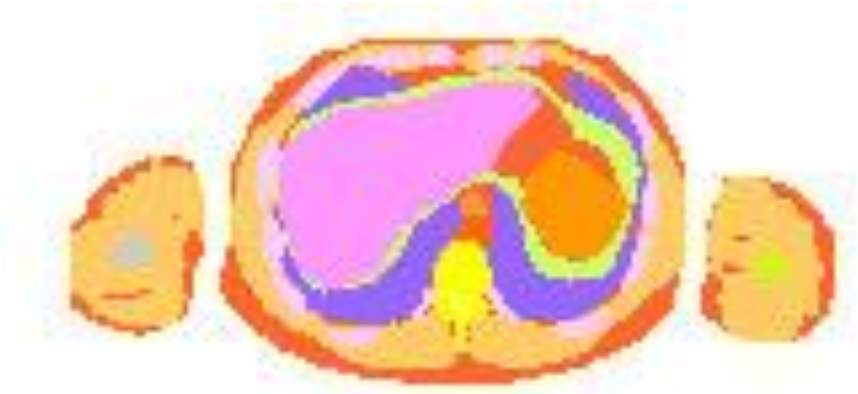

Figure 4. The MAX phantom: Sagittal view

Figure 5. The MAX phantom: Cut through MRI-head

2.3. Comparison with other phantoms

Table 4 also presents organ and tissue masses of the mathematical ADAM phantom (Kramer et al 1982a), and of the voxel phantoms VIPMAN (Xu et al 2000), NORMAN (Dimbylow 1995a) and GOLEM (Zankl and Wittmann 2001).

The data show correspondence as well as disagreement between single organ and tissue masses, total body weights and body heights among all phantoms. From this point of view it is impossible to see at least a vague relationship between single organ masses and total body weight and/or height.

Therefore a comparison was made for the mass of all critical soft-tissue organs together, which means for the sum of the masses of all organs listed in table 4 except for adipose, skeleton, muscle, red bone marrow, and skin. Table 5 shows the masses for this group of soft-tissue organs for the various phantoms, and it seems that ca. 7 kg is a reasonable weight for "reference-man-like" phantoms, whereas significant deviations from the Reference Man with regard to body weight and body height (VIPMAN) seem to be accompanied also by a higher mass for this group of soft-tissue organs.

Table 5. Total mass of the soft-tissue organs at risk

PHANTOM	ST-ORGANS
	[kg]
ICRP 23/70	7.2
ADAM	7.0
GOLEM	6.1
NORMAN	7.1
VIPMAN	9.1
MAX	6.9

However, instead of investigating this "7 kg-rule" further or carrying out extensive anatomical comparisons for organs and tissues from different phantoms, it seems to be more reasonable for the purposes of radiation protection to make dosimetric comparisons between various phantoms, something which has been done extensively in a recently published study by Zankl et al (2002a), for example.

3. The MAX phantom: Skeletal tissue masses

3.1. Skeletal tissues as specified by the ICRP

There is general agreement and also recognition by the IRCP (1991), that within the human skeleton the hematopoietic stem cells of marrow (active or red bone marrow) and the osteogenic cells on the endosteal surface of bone are at radiological risk for induction of leukemia and bone cancer, respectively.

According to ICRP Publications No. 23 (1975), 30 (1979), and 70 (1995) the skeleton is composed of bone, fatty or yellow bone marrow (YBM), active or red bone marrow (RBM) and connective tissue, like cartilage, periarticular tissue, etc.

There are two types of bone in the skeleton. Cortical or hard, compact bone found mainly in the shafts of the long bones. Trabecular or soft, spongy bone distributed in the interior of the flat bones and the ends of the long bones. Trabecular bone consists of a system of small cavities of irregular form and shape, filled with bone marrow, and with typical linear dimensions between 100 – 1700 micron (Beddoe et al 1976).

ICRP (1979) assumes a uniform distribution of RBM in the marrow cavities of trabecular bone, and that the equivalent dose to RBM can be estimated as the average equivalent dose in the cavities, which also may contain YBM. As for the osteogenic cells on the endosteal surface of bone, ICRP (1979) recommends that the equivalent dose be averaged over all tissues up to a distance of 10 micron from endosteal surfaces of cortical and trabecular bone.

In order to judge or change the representation of tissues in the phantom's skeleton, certain recommendations given in ICRP70 are helpful.

Table 6. Tissue distribution in the ICRP70-skeleton

TISSUE	MASS	DENSITY	VOLUME	VOLUME
	g	g/cm**3	cm**3	FRACTION
BONE	5500	1.92	2864.6	0.370
RED BM	1170	1.03	1135.9	0.147
YELL BM	2480	0.98	2530.6	0.327
CARTILAGE	1100	1.10	1000.0	0.129
MISC.	250	1.20	208.3	0.027
TOTAL	10500		7739.4	1.000

Column 2 and 3 of table 6 show the skeletal tissue masses and their mass fractions, respectively as recommended by ICRP70 for the adult Reference Male, who has a total body weight of 73 kg and is 176 cm tall. "MISC." includes the teeth, the periosteum, and blood vessels. The densities were taken from ICRU44 for the first four tissues. For the tissues of "Miscellaneous" masses and densities were found in ICRP70 and ICRP23, which allowed for an estimate of the combined density. Column 4 presents the corresponding tissue volumes and the last column shows the volume fractions.

Table 7. Cellularity factors and percentage mass fraction of RBM from ICRP70

Specific Bone	Cellularity Factor	RBM mass [%]
Lower Arms	0	0
Upper Arms	0.25	2.3
Ribcage*	0.60	22.8
Spine/Sacr.	0.70	42.2
Skull/Mand.	0.38	8.4
Pelvis	0.48	17.5
Upper Legs	0.25	6.7
Lower Legs	0	0

* Ribs,sternum,clavicles,scapulae

With regard to the distribution between RBM and YBM within different bones of the skeleton, ICRP70 recommends age-dependent, bone-specific cellularity factors, which represent the percentage of bone marrow volume occupied by the hematopoietic cells of the RBM. Table 7 shows the cellularity factors for the adult male together with the bone-specific, percentage mass fraction of RBM, which have also been specified in ICRP70.

3.2. The VOXTISS8 skeleton

The VOXTISS8 skeleton has a volume of 7867.7 cm^3, of which 1385.4 cm^3 have been segmented as "bone marrow", thereby representing only 17.6% of the total skeletal volume. The bone marrow of the ICRP70 skeleton (table 6) in contrast represents 47.4% of the total volume. As a result, with 13831.3 g the total weight of the VOXTISS8 skeleton is too heavy (table 3) for a person with a body height of 175.3 cm. Therefore, only for this quantitative argument the original segmentation of "bone marrow" cannot serve for a reasonable representation of skeletal tissues. But there is also a conceptual argument against this segmented volume of "bone marrow", namely the ratio between the voxel dimension, which is 0.36 mm (the original pixel side length of the scanned images was even 4 mm), and the marrow cavity dimensions, which can be less than 100 microns. It is simply impossible to segment any object with a pixel size which is greater than the object's linear dimension.

After the addition of the missing parts of the clavicles, the total skeletal volume of the VOXTISS8 phantom became 7915.4 cm^3 , which is 176 cm^3 or 2.3% more than the skeletal volume of the Reference Man (table 6). This is probably due to the fact that arms and legs have been added from the Visible Human Male, who has a body weight of 104 kg and a body height of 186 cm. After all, at least the total volume of the VOXTISS8 phantom can serve as a basis for the MAX skeleton, for which a new marrow distribution had to be found.

3.3. Representation of skeletal tissues in the MAX skeleton

An appropriate representation of skeletal tissue in the MAX phantom should reflect its anatomical peculiarities and at the same time the specific recommendations given by ICRP70. The method applied here will first estimate reasonable volumes for the RBM and the YBM. Then a specific technique, the CT number method, will be used to determine a voxel-specific distribution of bone marrow, taking into account the grey values of the skeletal pixels in the CT images of the scanned patient, as well as the RBM mass fractions and the cellularity factors as recommended by ICRP70 for the Reference Adult Male. These calculations will also produce an average density and the total weight of the MAX skeleton.

The volume of a skeleton with a tissue distribution based on ICRP70 (table 6) contains ca. 15.6% of cartilage plus "Miscellaneous" tissues. During the segmentation of CT images cartilage is usually segmented sometimes as part of bone and sometimes as part of skeletal muscle in order to achieve smooth surfaces between the skeleton and the surrounding muscle tissue. This also happens with the periosteum and the connected blood vessels, which are mostly located on the surface of bone. It was therefore decided to include only half of that volume, or 7.8%, in the skeletal tissue distribution of the MAX skeleton. The teeth, representing only 0.3% of the total skeletal volume, are already part of the segmented skeletal volume, and have therefore been neglected for further explicit considerations here.

<u>Volumes and Masses of skeletal tissues</u>

With the volume fractions and densities from table 6, the volumes and masses of the RBM and the YBM of the MAX skeleton can now be calculated as

Vol(RBM) = 7915.4 cm^3 x 0.147 = 1163.6 cm^3 ; Mass(RBM) = 1163.6 cm^3 x 1.03 g cm^{-3} = 1198.5 g

Vol(YBM) = 7915.4 cm^3 x 0.327 = 2588.3 cm^3 ; Mass(RBM) = 2588.3 cm^3 x 0.98 g cm^{-3} = 2536.6 g

<u>Voxel-specific distribution of bone marrow</u>

After a method introduced by Zankl and Wittmann (2001) the information held by the CT numbers (= grey values) of the skeletal pixels in the CT images of the scanned patient can be used to design a voxel-specific distribution of bone marrow. The CT number reflects the attenuation properties of the skeletal mixture contained in the corresponding voxel, which can be bone, or bone marrow, or a mixture of bone

and bone marrow, and it is obvious that low CT numbers mean that the voxel contains more marrow, while high CT numbers represent mainly bone.
In the first step the CT number method assigns the medium 'bone' to all skeletal voxels.
Then the range of skeletal CT numbers is separated into three parts:

- CT numbers up to a lower limit represent marrow,
- CT numbers above an upper limit represent bone, and
- Intermediate CT numbers (between the two limits) represent mixtures between bone and marrow.

According to its CT number, bone, or marrow, or a mixture of them is assigned to each skeletal voxel, and as far as the intermediate range is concerned the specific mixture is assigned to the voxel by linear interpolation between the lower and the upper limit. For this purpose a certain number of homogeneous skeletal mixtures of bone and marrow are defined and linked to corresponding CT number ranges between the limits. Consequently the skeleton becomes heterogeneous because each bone voxel gets a skeletal tissue composition according to its CT number, thereby reflecting the specific composition of bone and marrow it contains. Zankl and Wittmann assume that in bones, which contain RBM, the marrow volume per voxel is composed of RBM and YBM in equal parts, and that the skeletal voxels do not contain any cartilage or soft-tissue other than bone marrow.

This method is capable of producing a heterogeneous tissue distribution throughout the skeleton based on the CT numbers of the scanned person, and therefore represents an advantage compared to the earlier MIRD-5 marrow representation, which assigned one and the same homogeneous skeletal mixture to all bones of the skeleton.

Yet the crucial point for the CT number method to work, is the definition of the CT numbers for the lower and the upper limit, respectively. As CT numbers reflect only certain mixtures between bone and marrow contained in a voxel, they cannot reveal the absolute mass or volume of bone marrow in a specific voxel, or in a specific bone, or in the whole skeleton, and consequently also not the values for the lower and upper limit. Therefore it is necessary to "tell" the CT number method the total amount of marrow mass to be distributed among all skeletal voxels, and how to distribute this marrow mass among specific bones. In other words, the values for the lower and for the upper CT number limit are defined in such a way that a predefined RBM mass, for example, gets distributed among the skeletal voxels according to the CT numbers of skeletal voxels found in the images of the scanned person, and according to other criteria, like ICRP70 RBM mass fractions and cellularity factors.

<u>The CT number method as applied to the MAX phantom</u>.
The application of the CT number method requires access to the original CT images, which once served as a basis for the segmentation of the voxel phantom. Unfortunately there are no directly corresponding original CT images for the MAX phantom. As pointed out above there are two limited sets of CT images from the head and the trunk including a part of the upper arms and the upper legs of the patient, whose images served for the construction of the VOXTISS8 phantom. As for the main skeletal tissue at risk, the RBM, this limitation does not pose a problem, because the bones of the lower extremities contain only YBM, which is not considered a tissue at risk.

Unfortunately during the scanning of the trunk the patient was asked to raise the arms above his head. Consequently the position of the upper part of the upper arm bones on the original CT images do not match with their position in the segmented images of the MAX phantom, because there the arms are straightened downwards along the sides of the body. It was therefore decided to assign initially a medium CT number of 110 to all upper arm bone voxels, and also to the voxels of the added part of the clavicles, because the original CT images did not show these bones. This should not severely hamper the application of the CT number method because the RBM in the upper parts of the upper arm bones amounts to only 2.3%, and in the clavicles to only 0.8% of the total RBM mass, respectively, and this initial assignment can be preliminary, like the initial mixture composition in all other skeletal voxel too, because their tissue composition would be changed anyway, if the resulting bone-specific mass fraction deviates significantly from the ICRP70 fractions of table 7.

55 original CT images from the head and 78 original CT images from the trunk with CT numbers between 0 and 255 have been downloaded from the YALE homepage (Zubal 2001), have been resampled to achieve the 158×74 pixel format of the segmented MAX images, and have sometimes been repeated in order to produce a total number of 261 skeletal CT number images, which were necessary to correspond to the 261 segmented images of the MAX phantom, which cover the range from head to mid-thigh. The CT number data set constructed in this way can be considered as a sub-matrix for the bones already defined in the phantom's main matrix.

Table 8. Linear interpolation table for the distribution of RBM in the MAX skeleton based on the CT number method

SKELETAL. TISSUE	DENSITY g/cm**3	CT-NUMBER RANGE	BONE VOLUME FRACTION	RED BONE MARROW VOLUME FRACTION
Bone/Cart/M	1.862	169 - 255	1 - 0.078	0.00
9	1.830	158 - 168	9 x 0.1 x (1-0.078)	1 x CF/10 x (1-0.078)
Mixtures	1.739	147 - 157	8 x 0.1 x (1-0.078)	2 x CF/10 x (1-0.078)
of	1.649	136 - 146	7 x 0.1 x (1-0.078)	3 x CF/10 x (1-0.078)
trabecular	1.559	125 - 135	6 x 0.1 x (1-0.078)	4 x CF/10 x (1-0.078)
bone,	1.469	114 - 124	5 x 0.1 x (1-0.078)	5 x CF/10 x (1-0.078)
bone	1.378	103 - 113	4 x 0.1 x (1-0.078)	6 x CF/10 x (1-0.078)
marrow	1.288	92 - 102	3 x 0.1 x (1-0.078)	7 x CF/10 x (1-0.078)
and	1.198	81 - 91	2 x 0.1 x (1-0.078)	8 x CF/10 x (1-0.078)
cartilage/M	1.107	69 - 80	1 x 0.1 x (1-0.078)	9 x CF/10 x (1-0.078)
Bone Marrow	1.017	0 - 68	0.00	10 x CF/10

CF: Cellularity Factor
M: Miscellaneous tissues

After the phantom's main voxel matrix has been read by the transport code, the program reads the skeletal CT number data set, and assigns correspondingly one of the skeletal tissue mixtures to each bone voxel, based on a linear interpolation between CT number ranges as shown in column 3 of table 8. Based on this information volume fractions of RBM and bone are calculated as a function of the CT number range as shown in column 4 and 5, always taking into account the cellularity factor CF, but the 7.8% of cartilage plus other tissues only in bone and bone/marrow voxels. The YBM volume is calculated correspondingly with a factor of (1-CF), but not shown in table 8. If the resulting distribution of RBM among the bone deviates significantly from the ICRP70 data given in table 7, the mixture distribution of the skeletal voxels is changed until better agreement is achieved.

With a lower CT number limit of 68 and an upper CT number limit of 169 it was possible to distribute the pre-calculated 1198.5 g of RBM heterogeneously throughout the MAX skeleton with the resulting mass fractions as shown in table 9, which differ from the ICRP70 mass fractions on the average by 3% for the bones with more than 80% of the RBM (ribcage, spine and pelvis). The average skeletal density calculated by this procedure turned out to be 1.41 g cm^{-3} , and consequently the total weight of the MAX skeleton became 11146.5 g.

3.4. Comparison with other phantoms

ICRP70 recommends an average density of 1.3 g cm^{-3} for the skeleton, while on the other hand the data for the ICRP70 skeleton from table 6 would suggest also a value of 10500 g / 7739.4 cm^3 = 1.36 g cm^{-3} . ICRP23 (ICRP 1975) recommends 1.4 g cm^{-3} , whereas ICRP23-revised (ICRP 2001) adopts the 1.3 g cm^{-3} from ICRP70.

The average skeletal densities of the other phantoms are 1.45 g cm^{-3} for GOLEM (Zankl 2002b), and 1.49 g cm^{-3} for NORMAN (Jones 1997). Information about VIPMAN´s average skeletal density was not available. The total skeletal weights for all phantoms seem to relate reasonably well to their body heights, with the exception of VIPMAN. Compared with the other phantoms, 11245 g seem to be a relatively low skeletal weight for somebody who is 186cm tall and weighs 104 kg. According to the draft of ICRP23-revised, 20% of adipose-free total body mass can be considered as a reasonable estimate for the total weight of the skeleton, which would suggest rather 13590 g for the VIPMAN´s skeleton. A criterion to compare RBM data from different phantoms could be the mass fraction of RBM with respect to the total skeletal mass, which is 0.111 according to ICRP70 (table 6). For the phantoms considered here the following total RBM-mass fractions have been determined:

MAX = 0.108, GOLEM = 0.113, NORMAN = 0.139, VIPMAN = 0.100, and ADAM = 0.147 .

Table 9. Percentage mass fractions of RBM for the ICRP Reference Male and various phantoms

	ICRP70	MAX	GOLEM	VIPMAN	NORMAN	ADAM
	[%]	[%]	[%]	[%]	[%]	[%]
Low. Humeri	0	0	0	0	0	0
Upp. Humeri	2.3	3.6	5.8	3.6	2.3	1.9
Ribcage*	22.8	23.0	25.4	23.3	22.8	16.6
Spine/Sacr.	42.2	42.7	29.8	36.6	29.9	28.4
Skull/Mand.	8.4	7.7	8.1	4.5	8.3	13.1
Pelvis	17.5	16.3	19.7	28.0	33.4	36.2
Upp. Femur	6.7	6.7	11.1	3.9	3.3	3.8
Low. Femur	0	0	0	0	0	0
Total	99.9	100.0	99.9	99.9	100.0	100.0

* Ribs, sternum, clavicles ,scapulae

Table 9 shows also the bone-specific RBM mass fractions for the voxel phantoms GOLEM, VIPMAN, and NORMAN, as well as for the mathematical phantom ADAM. With regard to the major RBM containing bones, the ribcage, the spine, and the pelvis, there is reasonable agreement between ICRP70 and all voxel phantoms only with regard to the ribcage. This agreement still holds for the RBM mass fraction in the pelvis of GOLEM, whereas its spine contains 12% less RBM than recommended by ICRP. In case of the VIPMAN and NORMAN voxel phantoms many RBM mass fractions other than for the ribcage are significantly different from the ICRP70 fractions. While the RBM distributions in the MAX and in the GOLEM phantom have been determined by almost the same calculation method based on CT numbers, the RBM distribution for the VIPMAN phantom has been derived from the redness in certain areas of bone tissue visible in the color photographs of the Visible Human Male. The mass fractions for the NORMAN voxel phantom and for the mathematical ADAM phantom are simply outdated, because they reflect basically the old ICRP23 RBM mass fractions, which are meanwhile superseded by the ICRP70 data. The dosimetric implications of these differences will be discussed in the next chapter.

As for the osteogenic cells on the endosteal surface of bone (= bone surface in table 1) no attempt was made to design a special dosimetric model for calculating eqiuvalent dose in the 10 micron layer on the surfaces of cortical and trabecular bone. As before in the case of the mathematical ADAM and EVA phantoms, equivalent dose to the bone surface is estimated conservatively by the average equivalent dose to the skeleton.

4. Conversion coefficients for external exposures to photons

4.1. The MAX/EGS4 exposure model

The computational exposure model developed for this study consists of the MAX phantom coupled with the EGS4 Monte Carlo code (Nelson 1985).

The phantom file with the segmented images contains ca. 5.7 million cubic shaped voxels with linear dimension of 0.36 cm, corresponding to a voxel volume of 0.0467 cm^3. These voxels are distributed within a three-dimensional matrix made of 487 consecutive images of body cross-sections from head to toe, each of which is a two-dimensional matrix of 158 pixel times 74 pixel. Each voxel has its specific position within the three-dimensional matrix and has therefore a specific organ identification (ID) number assigned to it by segmentation, which explains of which organ or tissue the voxel is part of. The compressed form of this phantom voxel matrix has a size of about 4 Mb, while the sub-matrix with the CT numbers (= grey values) for the skeleton comprises ca. 1.4 Mb.

Import of the phantom file into the EGS4 code takes place through a subroutine, which reads the position and organ ID number of each voxel, in order to build the three-dimensional voxel matrix within the cartesian coordinate system of the Monte Carlo code. The dimensions of this imported matrix are 158 x 0.36 cm = 56,9 cm in the x-direction, 74 x 0.36 cm = 26.6 cm in the y-direction, and 487 x 0.36 cm =

175.3 cm in the z-direction. Figure 6 shows the surface of the MAX phantom and its orientation within the cartesian coordinate system.

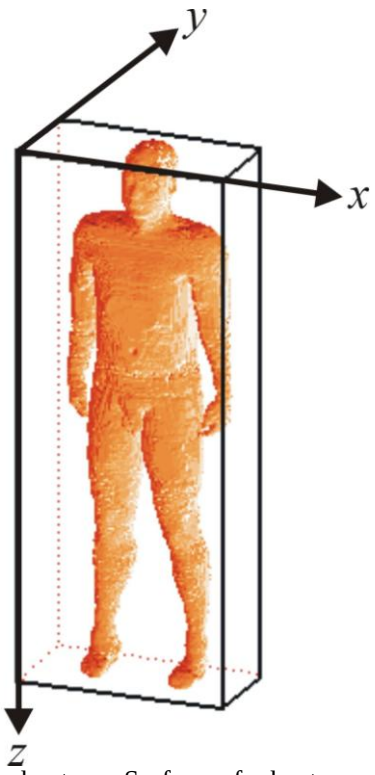

Figure 6. The MAX phantom: Surface of phantom and its position in the cartesian coordinate system

During this process a second ID number is assigned to each voxel which characterizes the material it contains. Consequently each voxel is clearly defined by its position and the two ID numbers for organ and material, respectively. Then import and evaluation of the CT number sub-matrix takes place as described in chapter 3.

The EGS4 system is a well-established and well-benchmarked Monte Carlo code for electron-photon-showers. In order to get photons and electrons transported through the voxel matrix a main code and two subroutines, called HOWFAR and AUSGAB, have been written according to the rules set out in the EGS4 user manual (Nelson 1985). HOWFAR passes information about the voxel geometry to the EGS4 code, while AUSGAB registers energy depositions in organ and tissue bins. Effective use of the transport algorithm requested the creation of an internal EGS4-matrix, in which all voxels are sequentially numbered from 1 to 5694004 instead of each voxel having three numbers for the x-, y- and z-direction, respectively. The code functions alternating between the two matrices depending on the task to be resolved: Monte Carlo radiation interaction processes take place in the internal sequential EGS4-matrix, while voxel geometry checks in HOWFAR and energy deposition per organ in AUSGAB happen in the cartesian voxel matrix. Energy lost by a particle in a specific voxel is deposited in the corresponding organ or tissue bin based on the ID number. Division by the organ's mass gives the average absorbed dose in the organ or tissue, which is numerically equal to equivalent dose for photons and electrons. All equivalent doses are calculated based on the sum of the energy deposited in all voxel which belong to the specific organ or tissue with the exception of the skin equivalent dose. As explained earlier equivalent dose to the skin is calculated only within the first 1.3 mm of skin tissue.

For external photon exposure the calculated equivalent doses are printed out as CCs normalized to incident fluence and to air-kerma free in air at the position of the phantom. The incident fluence is given by the number of photons and the field size used in the Monte Carlo run, which in turn can be converted into air-kerma by a tabulated conversion factor given as function of energy (ICRP 1996).

Normalization of organ equivalent dose to personal dose is also possible because an individual detector has been introduced to the surface of the MAX chest.

Conversion coefficients for different areas of radiation protection, for various types of radiation and for many field geometries have already been, or will be calculated with the MAX phantom. The complete data sets will be published in various papers and on a special website, whose address still has to be announced. For the completion of this article the following sections will present basic photon conversion coefficients for the RBM and Effective Dose.

4.2. Equivalent dose to the red bone marrow (RBM)

Weighting and correction factors

Having achieved a voxel-specific distributions of RBM, YBM, bone and cartilage/misc. in the MAX phantom as described in chapter 3, one should however not forget that the photon energy deposited in a voxel containing a homogeneous mixture has to be distributed among its components at least according to their mass fractions, a method which has already been applied to the early MIRD-type phantoms. In addition, for photon energies below 200 keV, for the calculation of absorbed dose to the RBM within a mixture of bone and marrow, the energy deposited

- has yet to be weighted with the ratio between the mass-energy-absorption (MEA) coefficients of RBM and the mixture, and
- has yet to be multiplied by the so-called "SPIERS-factors", which take into account the enhancement of absorbed dose to the RBM in trabecular cavities of specific bones due to the release of photoelectrons in adjacent bone entering the RBM cavity.

Rosenstein (1976) and independently Kramer (1979a) introduced these two energy-dependent factors, which are based on the data of Hubbell (1982) with regard to the MEA coefficients (figure 7), and with regard to the "SPIERS-factors" (figure 8) on the data of Spiers (1963b, 1968), who, together with his colleagues from the University of Leeds, did practically all the pioneering work on skeletal dosimetry from the forties to the eighties of the last century. Both factors depend on the energy of the photon before it collides with an electron in the homogeneous mixture.

This method of RBM equivalent dose calculation for external photon exposures has already been applied to the gender-specific mathematical phantoms ADAM and EVA, and their CCs have widely been published, also in ICRP74 (1996) and ICRU57 (1998).

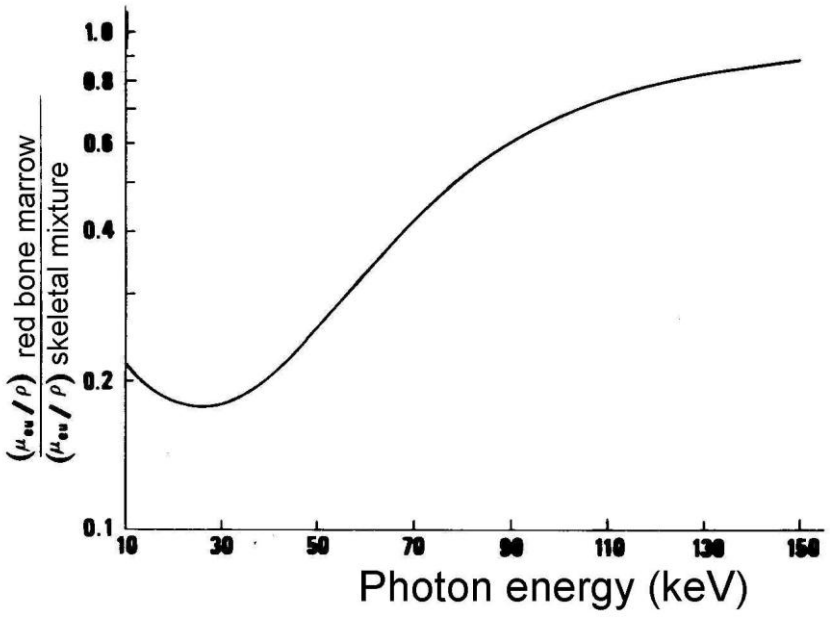

Figure 7. Ratio between mass-energy absorption coefficients for RBM and for the skeletal mixture as function of photon energy as used in the ADAM/EVA phantoms. From Kramer (1979b)

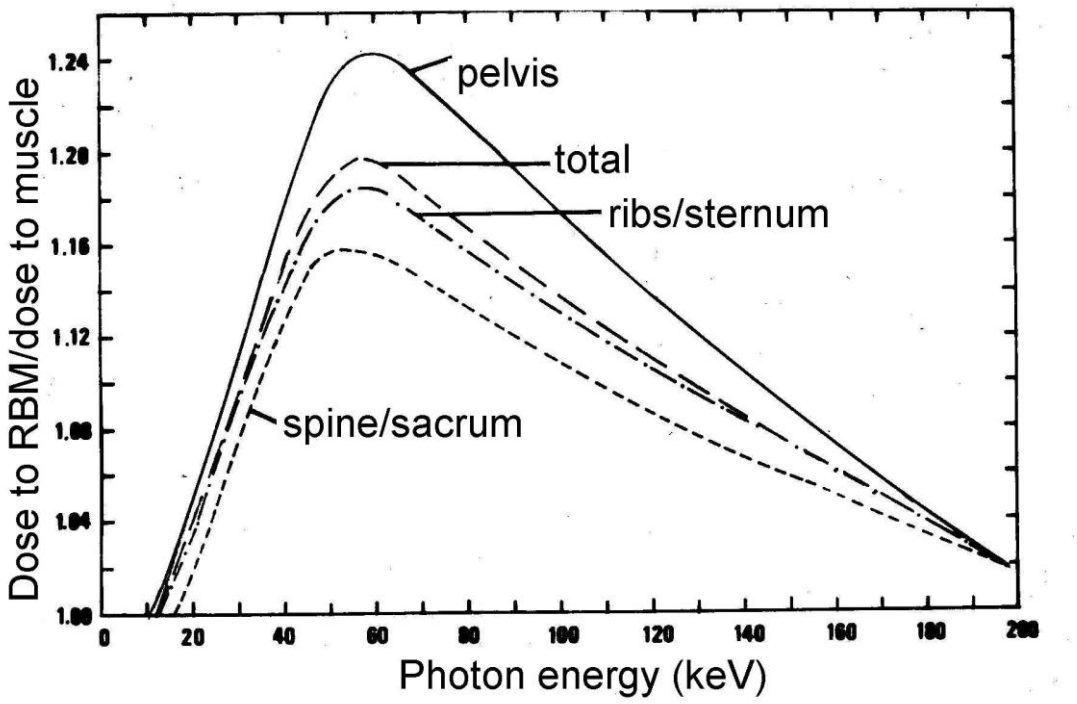

Figure 8. SPIERS-factors: Dose enhancement to RBM in trabecular cavities due to photoelectrons released in adjacent bone. From Kramer (1979b)

Basically the same method to calculate equivalent dose to the RBM has been applied to those skeletal voxels of the MAX phantom, which contain a mixture of bone and marrow. But now the ratio of the MEA coefficients is calculated for each voxel separately according to the specific mixture it contains, and as for the dose enhancement by photo-electrons released in adjacent bone, now new "KING-SPIERS-factors" (figure 9) are being applied. They are based on a more recent study from King and Spiers (1985), which show in general lower values for the bones already mentioned in figure 8, but a new, significantly greater correction factor for the skull.

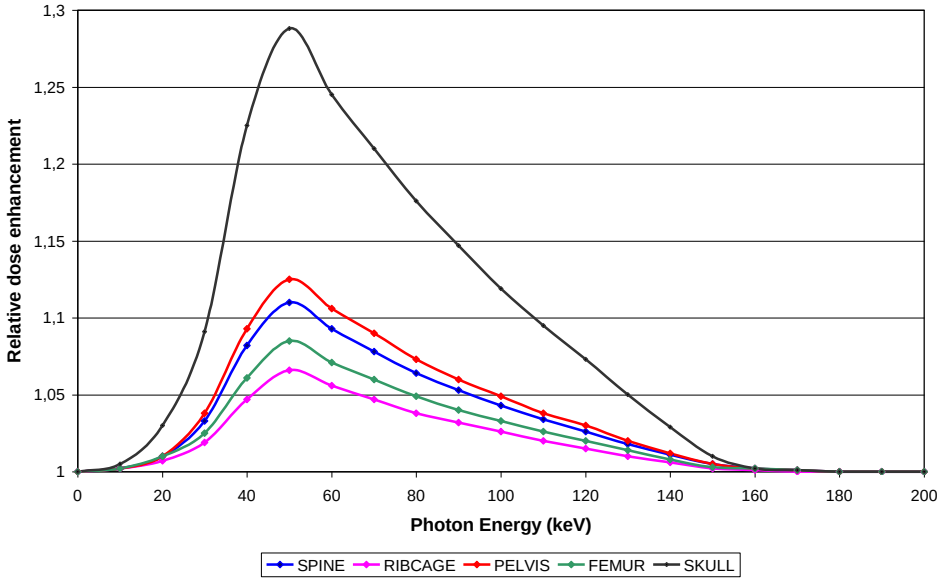

Figure 9. KING-SPIERS-factors: Dose enhancement to RBM in trabecular cavities due to photoelectrons released in adjacent bone

Results

RBM equivalent dose CCs have been calculated for external, broad, parallel beams of photons with energies from 10 keV to 10 MeV incident on the MAX phantom from the front (AP) and from the back (PA). Rayleigh scattering was included in the simulations, and the cut-off energy for the photons was 2 keV. Secondary electrons have not been considered. The results are presented as average equivalent dose normalized to air-kerma free in air as function of photon energy for AP- and PA-direction, respectively, and for comparison corresponding CCs for the voxel phantoms GOLEM (Zankl et al 2002c), and VIPMAN (Chao et al 2001a), and for the mathematical ADAM phantom (Zankl et al 1997) have been added to the figures. For all phantoms the coefficients of variance were around 1%.

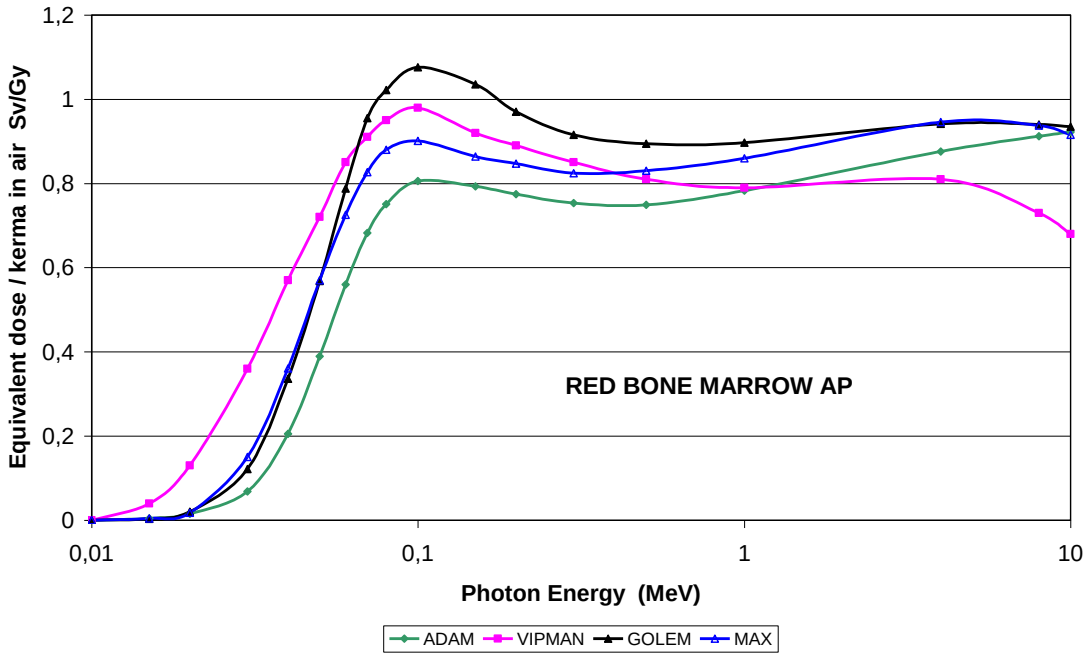

Figure 10. Conversion coefficients between RBM equivalent dose and kerma in air free in air as for external exposure to photons as function of energy for the MAX, GOLEM, VIPMAN, and ADAM phantom: AP incidence

AP incidence

Although both, MAX and GOLEM, use the CT number method to model the RBM distribution throughout the skeleton, their CCs (figure 10) are significantly different between 60 keV and 1 MeV. The MAX skeletal model uses the KING-SPIERS-factors (figure 9) and the ICRP70 cellularity factors (table 7), whereas the GOLEM skeletal model applies the SPIERS-factors (figure 8) and assumes equal volume fractions for RBM and YBM in the bones. In order to investigate the effect of these differences on RBM equivalent dose, two additional variations of the MAX skeletal model have been made:

- MAXS, which uses the older SPIERS-factors instead of the newer KING-SPIERS-factors, and
- MAXS5, which additionally assumes equal volume fractions for RBM and YBM.

The MAXS5 model corresponds to the GOLEM skeletal model, and as can be seen from figure 11, the two CCs are quite similar. However the introduction of the cellularity factors (MAXS5 → MAXS) leads to a first decrease of the RBM CC. The skull, the arm and leg bones, which usually receive a relatively high equivalent doses, contain now significantly less RBM, and the spine with 70% of RBM in the marrow volume is substantially shielded by overlying tissues for AP incidence. GOLEM has 6.6% more RBM in the long bones (table 9), which also contributes to this situation.

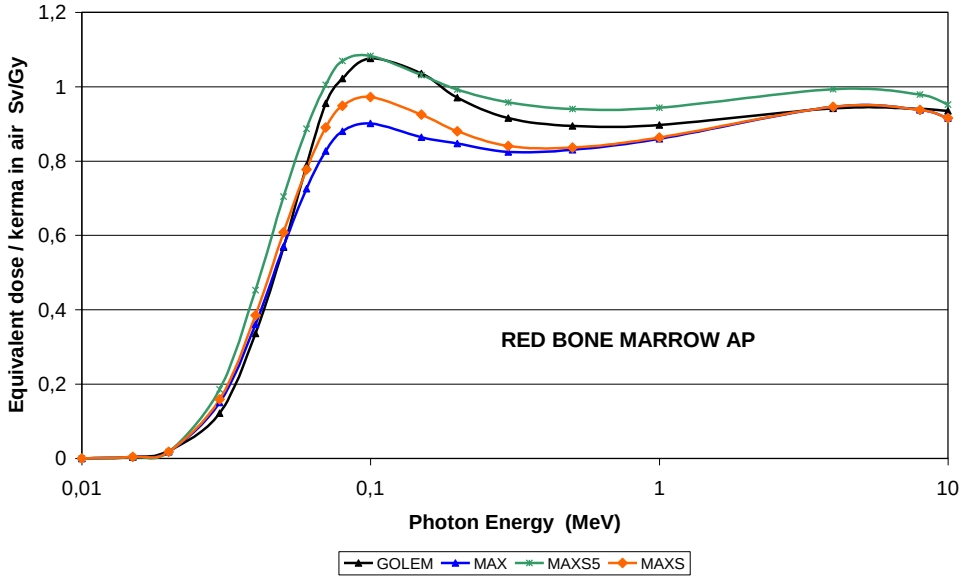

Figure 11. Conversion coefficients between RBM equivalent dose and kerma in air free in air as for external exposure to photons as function of energy for the MAX, MAXS, MAXS5 and GOLEM phantom: AP incidence

The introduction of the KING-SPIERS-factors (figure 9) (MAXS → MAX) leads to a second decrease of the RBM CC, because even the relatively high correction factor for the skull cannot compensate for the significantly lower factors for all other bones compared to the older SPIERS-factors (figure 8). Low RBM content in the ribcage and the long bones, high RBM content in the pelvis, and exaggerately backward positioned pelvis and spine are the reasons for the ADAM RBM CC being the lowest of all CCs for AP incidence (figure 10). The CC for the VIPMAN phantom (figure 10) is significantly higher compared to all other CCs up to ca. 60 keV, lies then between the CCs of MAX and GOLEM up to ca. 500 keV, and is finally decreasing for higher energies even below the ADAM CC, which is probably due to the effect of the secondary electrons considered in the calculation.

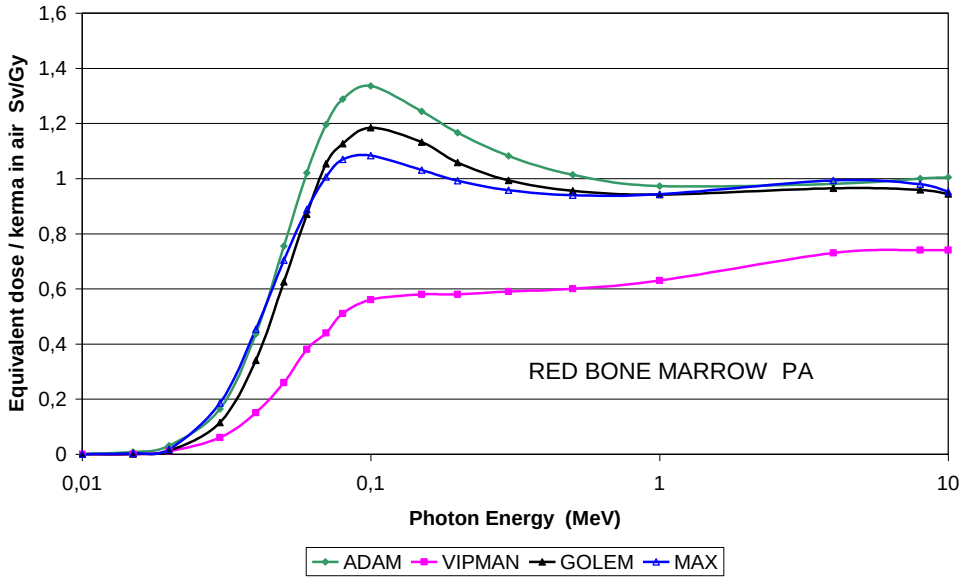

Figure 12. Conversion coefficients between RBM equivalent dose and kerma in air free in air as for external exposure to photons as function of energy for the MAX, GOLEM, VIPMAN and ADAM phantom: PA incidence

PA incidence

For PA incidence (figure 12) the decreasing effect of introducing the cellularity factors (MAXS5 → MAXS) is less pronounced mainly because of higher RBM volume (table 7) and RBM mass (table 9) in the spine of MAX compared to the spine of GOLEM, whereas the addition of the KING-SPIERS-factors (MAXS → MAX) again causes a significant decrease of the MAX RBM CC.

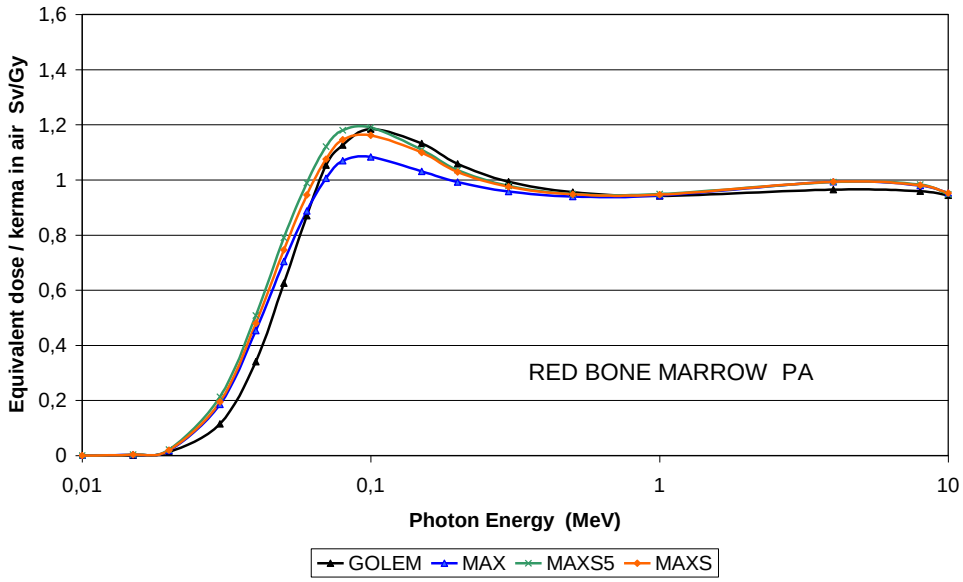

Figure 13. Conversion coefficients between RBM equivalent dose and kerma in air free in air as for external exposure to photons as function of energy for the MAX, GOLEM, VIPMAN, and ADAM phantom: PA incidence

It is not surprising that the ADAM RBM CC is now the highest (figure 13), because all factors mentioned before, which had a dose-reducing effect for AP incidence, function for PA incidence just in the opposite way.

MAX, GOLEM and ADAM have in common that the CC for PA incidence is higher than the CC for AP incidence, because of the anatomical distribution of bones in the trunk of the human body, and because of the distribution of RBM mass throughout the skeleton (table 9). It is therefore difficult to understand, why the VIPMAN CC for PA incidence (figure 13) is significantly lower (almost 50%) than the CC for AP incidence. This is even more surprising, because the pelvis of the VIPMAN contains substantially more RBM (table 9) than the pelvis of MAX or GOLEM, respectively. Also one would expect to see for PA incidence the same decrease of the CC for high energies due to the effect of secondary electrons as for AP incidence (figure 10).

The skeletal model of the VIPMAN phantom is quite different from the CT number models of MAX and GOLEM, which makes comparisons difficult. Although the authors (Chao et al 2001) recognize the difficulty to segment RBM in cavities having volumes in the range of 10^{-6} to 4.9 mm^3 with a voxel volume of 0.11 mm^3 , they nevertheless claim to have segmented RBM voxels by applying a threshold value to the redness of skeletal tissue (VIPMAN was segmented from color photographs), thereby deciding what is RBM and what is bone. It has to be assumed, that this procedure would segment in some parts of the skeleton spongiosa, which, according to ICRP70, is trabecular bone filled with marrow.

4.3. Effective Dose

Calculation of effective dose requires the determination of H_T as arithmetic average of the equivalent dose to tissue T for an adult male and for an adult female, respectively. Also it is understood that the tissue weighting factor for the breast applies to females only (Kramer 1982b,ICRU 1998).

In figures 14 and 15, only the CCs for ADAM/EVA represent the effective dose as defined by ICRP, because the equivalent doses to the organs and tissues at risk (table 1) have been calculated for an adult male phantom (ADAM) and for an adult female phantom (EVA), and then averaged and added as recommended in ICRU57 (ICRU1998).

As a female voxel phantom was not available for this investigation, it was decided to calculate an effective MAX dose. For this purpose the breasts , the ovaries and the uterus have been left out from the list of organs and tissues to be considered (table 1). The tissue weighting factors have not been re-normalized which means that their sum is 0.95. The gonad weighting factor of 0.2 was applied to the equivalent dose to the testes, and the remainder consisted of only 9 organs instead of 10.

The same concept has been used for the effective GOLEM dose. Effective VIPMAN dose has been calculated similar to this concept, except for the inclusion of male breasts. In case of the VIPMAN the breasts were two "thin layers of fat tissue around the chest level" (Chao et al 2001).

The NORMAN phantom (Dimbylow1995) was designed based on MRI data and later modified to match the old ICRP Reference Man data that is a body weight of 70kg and a body height of 170cm (ICRP1975). For the calculations performed by Jones (1997) for external photon exposures the NORMAN phantom was then modified a second time to match the new referential body height of 176 cm and weight of 73 kg. The phantom also has male breasts but no specification was found as to their design. The effective NORMAN dose cited in the figures has been determined similar to the other effective male doses.

A profound comparison of effective doses requests detailed information from each phantom about the anatomical parameters, the tissue compositions, the skeletal dosimetric model, etc., and knowledge of the equivalent doses to at least the first 10 organs and tissues mentioned in table 1. For the phantoms considered here, these data exist and were available, except for the organ and tissue equivalent doses of the NORMAN phantom. A presentation of only the first 10 organ and tissue equivalent doses for each phantom considered for the purpose of a comparative discussion of effective dose would however exceed a reasonable volume for this presentation. Therefore it is inevitable that the following discussion refers sometimes to data which are not presented here.

CCs for effective dose in terms of equivalent dose normalized to air-kerma free in air as function of photon energy for the mathematical phantoms ADAM and EVA, and for the voxel phantoms MAX, GOLEM, NORMAN, and VIPMAN are presented in figure 14 for AP-projection, and in figure 15 for PA-projection, respectively. The coefficients of variance were 1-2% for ADAM/EVA, GOLEM, MAX, and VIPMAN, and ca. 5% for NORMAN.

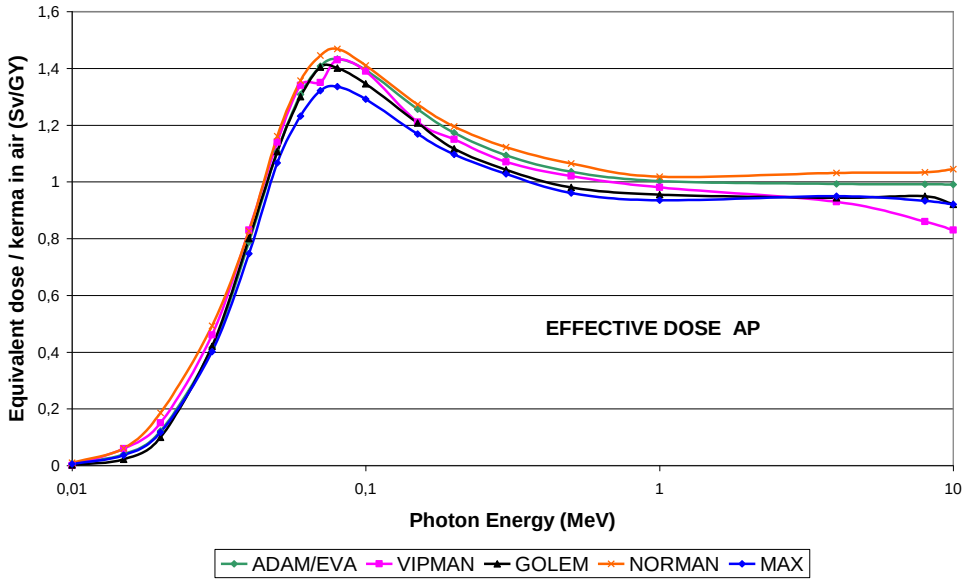

Figure 14. Conversion coefficients between effective dose and kerma in air free in air as for external exposure to photons as function of energy for the MAX, GOLEM, VIPMAN, NORMAN, and ADAM phantom: AP incidence

AP incidence

Reasonable agreement among the CCs for effective dose and all effective male doses can be observed for AP-projection in figure 14, except for the effective MAX dose being somewhat lower between 60 keV and 200 keV because of the lower RBM dose (figure 10), which contributes with a relatively high risk-weighting factor of 0.12 to effective MAX dose. However, due to the results shown in figure 11, and also because many organ equivalent doses of MAX and GOLEM agree reasonably well, it is possible that the effective GOLEM dose would approach the effective MAX dose, if the skeletal model for GOLEM would be updated with regard to the cellularity factors (table 7) and the KING-SPIERS-factors (figure 9). Although the RBM CC for ADAM/EVA is significantly lower than those for the other phantoms (figure 10), its effective dose CC is nevertheless quite high (figure 14). This is due to the fact that for the lungs, the stomach, the bladder, the breasts, the liver, and the thyroid the ADAM/EVA equivalent doses are almost always higher than the corresponding data of most of the other phantoms. The reasons can be found in anatomical differences between mathematically designed organs and true to nature anatomical representations, also because of higher female equivalent doses due to less shielding by muscle and adipose tissue, and because of the equivalent dose to the breast, which is included in the ADAM/EVA effective dose but not in the CCs for MAX and GOLEM. The CCs for VIPMAN and NORMAN are higher than those for MAX and GOLEM, which could reflect the inclusion of male breasts.

PA incidence

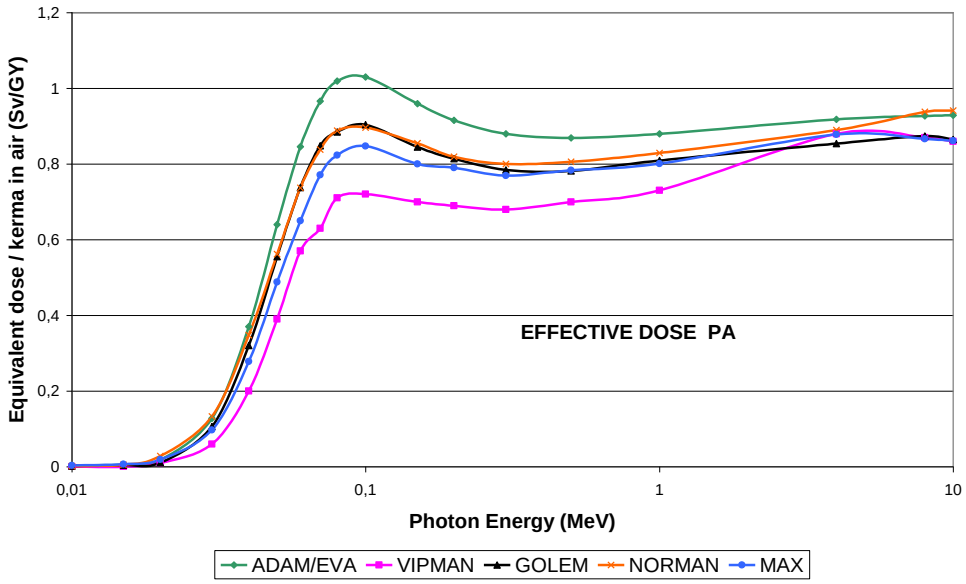

Figure 15. Conversion coefficients between effective dose and kerma in air free in air as for external exposure to photons as function of energy for the MAX, GOLEM, VIPMAN, NORMAN, and ADAM phantom: PA incidence

For the comparison between the effective MAX dose and the effective GOLEM dose (figure 15) the same arguments apply as already mentioned for the AP incidence. For PA incidence ADAM/EVA have significantly higher equivalent doses than MAX and GOLEM for the red bone marrow, the lungs, the liver, and the colon. Anatomical comparisons between ADAM/EVA and voxel phantoms have demonstrated that form and position of various organs and tissues of the mathematical phantoms do not represent very well human anatomy. Especially the skeleton and the lungs are located too much in the rear part of the trunk. Therefore and because of the pelvis-biased RBM distribution mentioned in the previous section, the effective dose is relatively high for PA incidence.

For PA incidence the VIPMAN effective dose (figure 15) is significantly lower, because equivalent doses to the testes, to the red bone marrow, to the colon and to the stomach are significantly lower than corresponding equivalent doses for the other phantoms. The VIPMAN phantom represents the

body of a person who was 186cm tall and weighed 104 kg. Possibly the substantial amount of additional muscle and adipose tissue (table 4) may have had a shielding effect on underlying soft-tissue organs like the colon and the stomach. Because of VIPMAN's closed thighs, the testes are shielded for PA incidence, which is not the case for MAX and GOLEM, and only in part in case of ADAM.

Because of the pelvis-biased RBM distribution of the NORMAN phantom (table 9) one would expect its CC for PA incidence to be closer to the ADAM/EVA CC. But the skeletal model of NORMAN uses already the KING-SPIERS-factors (figure 9), which cause significantly less dose enhancement to the RBM than the former SPIERS-factors (figure 8), which have been applied to ADAM/EVA.

5. Conclusions and perspectives

A Male Adult voXel (MAX) phantom has been developed, which corresponds reasonably to the specifications of the ICRP Reference Man with regard to body height, body weight, and the masses of the organs and tissues relevant in radiation protection. A sophisticated skeletal model based on the CT number method by Zankl and Wittmann (2000), on the MEA coefficients by Hubbel (1982) and on the photoelectron correction factors by KING and SPIERS (1985) has successfully been introduced into the phantom, in order to allow for a calculation of equivalent dose to the RBM.

A new computational exposure model, the MAX phantom connected to the EGS4 Monte Carlo code, has been designed, and CCs for 19 risk-relevant organs and tissues in terms of equivalent dose normalized to air-kerma free in air have been calculated as function of photon energy from 10 keV to 10 MeV for incidence of the radiation from the front and from the back and other field geometries.

Selected CCs for the RBM, and for effective MAX dose have been presented and comparatively discussed with regard to corresponding data from the adult phantoms ADAM/EVA , GOLEM, VIPMAN, and NORMAN.

From the data presented it can be concluded that the MAX/EGS4 exposure model can calculate equivalent dose data which fit reasonably well into the already existing data sets from other phantoms. It is to be expected that the data of MAX and GOLEM would agree better, if the skeletal model of GOLEM would be updated with regard to the cellularity factors and the newer KING-SPIERS-factors.

The RBM distribution of ADAM and EVA could also easily be updated with the ICRP70 RBM distribution, the cellularity factors, and the newer KING-SPIERS-factors. But then there is still the problem with the questionable anatomy of the skeleton and other organs. As the trend nowadays goes in the direction of voxel phantoms, it seems that a change of the anatomy of the MIRD-type phantoms does not recommend itself anymore.

Anatomically NORMAN agrees quite well with MAX, because both phantoms were designed to match the ICRP Reference MAN. The skeletal model applied to the NORMAN phantom is the same as used for ADAM and EVA with two exceptions: The RBM distribution is somewhat different from the MIRD-5 type phantoms but still pelvis-biased (table 9), and the correction for dose enhancement by photoelectrons released in adjacent bone is done with the newer KING-SPIERS-factors.

Unfortunately single organ equivalent doses for NORMAN were not available for this investigation, and therefore a precise examination of the effective NORMAN dose was not possible.

Compared with the other voxel phantoms, VIPMAN is much taller, much heavier, and has a completely different skeletal model compared with all other phantoms. Some differences can be explained, like the low PA testes equivalent dose because of shielding by the closed thighs, others not, like the low RBM equivalent dose for PA incidence.

The voxel structure of the true to nature CT images of real persons opens the prospect of skeletal Monte Carlo dosimetry in cavities of trabecular bone. The crucial factor for the realization is the voxel size, because in order to segment a certain tissue of the human body, the pixel size of the image has to be smaller than the typical linear dimensions of the object to be segmented. In the case of the bone marrow located in small cavities of trabecular bone, this would imply pixel resolutions in the range of some microns. Pioneering work in the area of nuclear medicine, performed mainly by a group centered at the University of Florida, has meanwhile indeed pushed Monte Carlo dosimetry to the level of the microscopic distribution of marrow in cavities of trabecular bone. Latest efforts presented Monte Carlo calculations with electrons in trabecular cavities of a micro-scanned specimen of bone estimating dose separately to the RBM and to the YBM, using a voxel size of 6.8×10^{-4} mm^3 (Bolch et al 2002).

The voxel size of the MAX phantom is 46.7 mm^3, of the GOLEM phantom 34.6 mm^3, of the NORMAN phantom 8 mm^3 , and of the whole body phantom with the actual finest resolution, the VIPMAN, still 0.11 mm^3 . Therefore, at least for these voxel phantoms, micro-skeletal Monte Carlo

dosimetry is out of question. Even if voxel volumes for whole body scans would arrive well below the size of trabecular cavities, one has still to be aware of the enormous number of voxels being produced by this resolution, and consequently of the memory requirements for the computer. But there are no principle arguments that would prohibit that these limitations will be surmounted one day.

As the development of the MAX phantom took place in various stages, all the data presented here exceed preliminary data published earlier (Kramer et al 2001, Kramer et al 2002a, Kramer et al 2002b, Vieira et al 2002a, Vieira et al 2002b, Lima et al 2002). According to the specific area of radiation protection, future publications will present results for other field geometries and types of radiation, as well as for internal exposures. It is the intention of the authors, that once these basic data have been published, to make the MAX phantom freely available for the scientific community on a special website.

6. Acknowledgement

The authors would like to express their gratitude to I.G. Zubal from the YALE University, New York for offering the VOXELMAN data to the scientific community. Thereby the construction of MAX was possible in the first place. For many helpful discussions and support the authors would like to thank also I. G. Zubal, X.G.Xu from the Rensselear Polytechnic Institute, Troy, New York, P.Dimbylow from the National Radiological Protection Board, Chilton, UK, and especially M. Zankl and N. Petoussi-Henss from the GSF research center for Umwelt und Gesundheit in Munich, Germany. The authors also would like to acknowledge the "Conselho Nacional de Desenvolvimento Científico e Tecnológico-CNPq" for the financial support.

References

Alderson, S W, Lanzl, L H, Rollins, M and Spira, J (1962) An instrumented phantom system for analog computation of treatment plans, Am. J. Roentg.87, 185

Alsmiller R G Jr. and Moran H S, (1968) Dose rate from high-energy electrons and photons, Nucl. Instr. Meth. 58,343-344

Alsmiller R G Jr, Armstrong T W and Coleman W A (1970), The absorbed dose and dose equivalent from neutrons in the energy range 60 to 3000 MeV and protons in the energy range 400 to 3000 MeV, Report ORNL-TM-2924 (rev.),Oak Ridge National Laboratory, Oak Ridge, Tenn., USA

Auxier J A, Snyder W S and Jones T D (1969), Neutron interactions and penetration in tissue, In: Attix F H and Roesch W C (eds.) Radiation dosimetry, 2nd ed.,Vol.1, pp.275-316, New York, Academic Press

Beck H L (1970), A new calculation of dose rates from high energy electrons and photons incident on 30 cm water slabs, Nucl. Instr. Meth. 78,333-334

Beddoe A H, Darley P J, Spiers F W (1976), Measurements of Trabecular Bone Structure in Man, Phys. Med. Biol., **21**, No.4,589-607

Berger M J and Seltzer S M (1969), Quality of radiation in a water medium irradiated with high energy electron beams, presented at the 12th International Congress of Radiology, Tokyo, 6-10 October, National Bureau of Standards, Washington, D.C., USA

Bolch W E, Patton P W, Rajon D A, Shah A P, Jokisch D W, Inglis B A (2002), Consideration Of Marrow Cellularity in 3-Dimensional Dosimetric Models of the Trabecular Skeleton, J Nucl Med, 43:97-108

Caon M, Bibbo G and Pattison J (1997), A comparison of radiation dose measured in CT dosimetry phantoms with calculations using EGS4 and voxel-based computational models, Phys. Med. Biol. 42:219-229

Caon M, Bibbo, G and Pattison, J. (1999), An EGS4-ready tomographic computational model of a fourteen-year-old female torso for calculating organ doses from CT examinations, Phys. Med. Biol. 44:2213-2225

Chao T C, Bozkurt A, Xu X G (2001a), Conversion Coefficients Based on the VIP-Man Anatomical Model and EGS4-VLSI Code for External Monoenergetic Photons from 10 keV to 10 MeV, Health Physics 81(2):163-183

Chao T C, Bozkurt A and Xu XG (2001b), Organ dose Conversion Coefficients for 0.1-10 MeV Electrons Calculated for the VIP-Man Tomographic Model. Health Physics 81(2):203-214

Cristy, M (1980) Mathematical phantoms representing children at various ages for use in estimates of internal dose, Report ORNL/NUREG/TM-367, Oak Ridge National Laboratory, Oak Ridge, Tenn., USA

Cristy M, Eckerman K F (1987), Specific Absorbed Fractions of Energy at Various Ages from Internal Photon Sources.ORNL/TM-8381 Vol. 1-7,Oak Ridge National Laboratory, Oak Ridge, Tenn., USA

Delafield H J (1963), Gamma-ray exposure in a man phantom related to personnel dosimetry, AERE-R 4430 Harwell, Atomic Research Establishment

Dimbylow, P J (1995a), The development of realistic voxel phantoms for electromagnetic field dosimetry, In: Proceedings of an International Workshop on Voxel Phantom Development held at the National Radiological Protection Board, Chilton, UK, 6-7 July

Dimbylow, P J editor (1995b), Voxel Phantom Development, Proceedings of an International Workshop held at the National Radiological Protection Board, Chilton, UK, on 6 and 7 July

Drexler G and Kramer R (1977), Relations between Metrological Quantities and Quantities Relevant in Radiation Protection for External Gamma Exposure, Paper SO 335, IV International Congress of Radiology, Rio de Janeiro

Fisher, H L and Snyder W S (1967), Distribution of dose in the body from a source of gamma rays distributed uniformly in an organ, Report No. ORNL-4168, Oak Ridge National Laboratory, Oak Ridge, Tenn., USA

Fisher, H L and Snyder W.S. (1968), Distribution of dose in the body from a source of gamma rays distributed uniformly in an organ, In: Proceedings of the First International Congress on Radiation Protection, Pergamon Press, Oxford, pp 1473-1486

Gibbs, S J, Pujol, A, Chen, T S, Malcolm, A W and James, A E (1984), Patient risk from interproximal radiography, Oral Surg. Oral Med. Oral Pathol., 58:347-354

Hubbell, J H (1982), Photon mass attenuation and energy-absorptions coefficients from 1 keV to 20 MeV, Int. J. Appl. Rad. Isot., **33**, 1269

ICRP (1973), Data for Protection against Ionizing Radiation from External Sources: Supplement to ICRP Publication No.15, ICRP Publication No.21, International Commission on Radiological Protection, Pergamon Press, Oxford

ICRP (1975), Report of the Task Group on Reference Man. ICRP Publication 23, International Commission on Radiological Protection, Pergamon Press, Oxford

ICRP (1979), Limits for intakes of radionuclides by workers. ICRP Publication 30.Intenational Commission on Radiological Protection, Pergamon Press, Oxford

ICRP (1987), Radiation Dose to Patients from Radiopharmaceuticals. ICRP Publication No.53 Pergamon Press, Oxford

ICRP (1991), 1990 Recommendations of the International Commission on Radiological Protection. ICRP Publication 60.International Commission on Radiological Protection, Pergamon Press, Oxford

ICRP (1994) Human repiratory tract model for rediological protection: a report of a Task Group of the
International Commission on Radiological Protection, ICRP Publication 66.
Pergamon Pess, Oxford

ICRP (1995), Basic Anatomical and Physiological Data for use in Radiological Protection: The Skeleton. ICRP Publication 70.International Commission on Radiological Protection, Pergamon Press, Oxford

ICRP (1996), Conversion Coefficients for use in Radiological Protection against External Radiation. ICRP Publication 74.International Commission on Radiological Protection, Pergamon Press, Oxford

ICRP (2001), Draft ICRP Report: Basic Anatomical and Physiological Data for Use in Radiological Protection: Reference Values, http://www.icrp.org/download_anatomical.htm

ICRU (1989), Tissue substitutes in radiation dosimetry and measurement. ICRU Report 44.International Commission on Radiation Units and Measurements, Bethesda, MD

ICRU (1992), Phantoms and Computational Models in Therapy, Diagnosis and Protection.
ICRU Report 48, International Commission on Radiations Units and Measurements, Bethesda, MD

ICRU (1998), Conversion coefficients for use in Radiological Protection against External Radiation. ICRU Report 57.International Commission on Radiation Units and Measurements, Bethesda, MD

Irving D D, Alsmiller R G Jr. and Moran H S (1967) Tissue current-to dose conversion factors for neutrons with energies from 0.5 to 60 MeV. Report ORNL-4032, Oak Ridge National Laboratory, Oak Ridge, Tenn., USA

Jones A R (1966), Proposed calibration factors for various dosimeter at different energies, Health Physics 12, 663

Jones D G (1997), A Realistic Anthropomorphic Phantom For Calculating Organ Doses Arising From External Photon Irradiation. Radiation Protection Dosimetry Vol.72, No.1, pp.21-29

Johnson, L, Ljundberg, M, Sjogreen, K, Strand, S E (2000), The conjugate view method: evaluation of activity and absorbed dose calculations from Monte Carlo simulated scintillation camera images using experimental data in an anthropomorphic phantom, J Nucl Med 41 (Suppl): 234P

King S D, Spiers F W (1985), Photoelectron enhancement of the absorbed dose from X rays to human bone marrow: experimental and theoretical studies, Br. J. of Radiol. **58**, 345-356

Kramer R (1979a), Ermittlung von Konversionsfaktoren zwischen Koerperdosen und Relevanten Strahlungskenngroessen bei Externer Roentgen- und Gamma-Bestrahlung,Gesellschaft fuer Strahlen- und Umweltforschung, Muenchen-Neuherberg, GSF-Bericht-S-556

Kramer R and Drexler G (1979b), Determination of Dose Equivalent for External Irradiation of Occupationally Exposed Personnel, In: IAEA Regional Seminar on Reducing Occupational Exposures to the Lowest Reasonably Achievable Levels, Athens, IAEA

Kramer R, Zankl M, Williams G, Drexler G (1982a), The Calculation of Dose from External Photon Exposures Using Reference Human Phantoms and Monte Carlo Methods. Part I: The Male (ADAM) and Female (EVA) Adult Mathematical Phantoms. GSF-Report S-885.Reprint July 1999.Institut fuer Strahlenschutz, GSF-Forschungszentrum fuer Umwelt und Gesundheit, Neuherberg-Muenchen

Kramer R and Drexler G (1982b), On the Calculation of Effective Dose Equivalent, Rad. Prot. Dos. Vol.3,No.1/2,p.13-24

Kramer R, Vieira, J W, Lima, F R A and Fuelle, D.(2001), An EGS4-based Monte Carlo code for the calculation of organ equivalent dose to a modified Yale voxel phantom, paper presented at the Symposium on New Trends in Biophysics, 23-26.9.2001, Recife, Brazil

Kramer R, Vieira J W and Lima F R A (2002a), MAX – A Male Adult voXel phantom for Monte Carlo calculations of internal and external exposures in radiation protection. Paper presented at the International Topical Meeting on Industrial Radiation and Radioisotope Measurement Applications, 9-14 June 2002, Bologna, Italy.

Kramer R, Vieira J W and Lima F R A. (2002b), MAX– A Male Adult voXel model for radiation protection dosimetry, ,paper presented at the VI National Meeting on Nuclear Applications – ENAN, 11-16.8.2002, Rio de Janeiro, Brazil

Ligot L, Diallo I, Shamsaldin A, Chavaudra J, BonaÎti-Pellié and Vathaire F (1998), Individualized phantom based on CT slices and auxological data (ICTA) for dose estimations following radiotherapy for skin haemangioma in childhood, Radiotherapy and Oncology 49,279-285

Lima, F R A, Kramer, R and Vieira, J W, (2002), Conversion coefficients for relevant body tissues for external photon exposures calculated for the EGS4-based MAX (Male Adult voXel) phantom, paper presented at the 5th International Topical Meeting on Industrial Radioisotope and Radiation Measurement Applications, Bologna, Italy, 9-14 June 2002

Nelson W R, Hirayama H, Rogers D W O (1985), The EGS4 Code System. SLAC-265 Stanford Linear Accelerator Center, Stanford University, Stanford, California

Petoussi-Henss N and Zankl M (1998), Voxel Anthropomorphic Models as a Tool for Internal Dosimetry, Rad. Prot. Dos. Vol.79, Nos 1-4, pp. 415-418

Petoussi-Henss, N, Zankl M, Fill U and Regulla D (2002), The GSF family of voxel phantoms, Phys. Med. Biol. 47:89-106

Rosenstein M (1976), Organ Doses in Diagnostic Radiology, (US Department of Health, Education and Welfare, Bureau of Radiological Health) BRH Tech. Publ., DA 76-8030

Saito K, Wittmann A, Koga S, Ida Y, Kamei T, Funabiki J, Zankl M (2001), Construction of a computed tomographic phantom for a Japanese male adult and dose calculation system. Radiat Environ Biophys 40: 69-76

Sidewell J M, Burlin T E and Wheatley B M (1969), Calculation of the absorbed dose in a phantom from photon fluence and some applications to radiological protection, Br. J. Radiol. 42, 522-529

Sidewell J M and Burlin T E (1973), Photon fluence calculations for estimating dose distribution in the thorax, Br. J. Radiol. 46,360-364

Sjogreen K (1998) In: The Zubal Phantom Data, Voxel-based Anthropomorphic Phantoms, http://noodle.med.yale.edu/phantom

Smith T, Petoussi-Henss N and Zankl M (2000), Comparison of internal radiation doses estimated by MIRD and voxel techniques for a "family" of phantoms. Eur J Nucl Med 27:1387-1398

Smith T, Phipps A W, Petoussi-Henss N and Zankl M (2001), Impact on Internal Doses of Photon SAFs Derived with the GSF Adult Male Voxel Phantom. Health Physics, Vol. 80 No.5 pp

Snyder W S (1950), Calculations for maximum permissible exposure to thermal neutrons, Nucleonics 6, 2, 46-50

Snyder W S (1965), The variation of Dose in Man from Exposure to a Point Source of Gamma Rays, Le Vesinet

Snyder W S (1971), Dose distribution in a cylindrical phantom for neutron energies up to 14 MeV, In: Protection against neutron radiation. NCRP Report No.38, pp.46-84, Washington, D. C., National Council on Radiation Protection and Measurements

Snyder W S, Ford M R, Warner G G, Watson G G (1974a), Revision of MIRD Pamphlet No. 5 Entitled "Estimates of absorbed fractions for monoenergetic photon sources uniformly distributed in various organs of a heterogeneous phantom". ORNL-4979, Oak Ridge National Laboratory, Oak Ridge, Tenn.

Snyder W S, Ford M R, Warner G G and Watson SB (1974b), A Tabulation of Dose Equivalents per Microcurie-Day for Source and Target Organs of an Adult for Various Radionuclides, Report ORNL-5000/TM-367,Oak Ridge National Laboratory, Oak Ridge, Tenn., USA

Snyder W S, Ford M R, Warner G G and Watson S B (1975), "S": absorbed dose per unit cumulated activity for selected radionuclides and organs. MIRD pamphlet No.11, New York: Society of Nuclear Medicine

Snyder W S, Ford M R and Warner G G (1978), Estimates of absorbed fractions for monoenergetic photon sources uniformly distributed in various organs of a heterogeneous phantom, MIRD Pamphlet No.5, revised, Society of Nuclear Medicine, New York N. Y.

Spiers F W (1956), Appendix J in: Hazards to Man of Nuclear and Allied Radiations, Cmd 9780, H. M. S. O. London

Spiers F W and Overton T R (1963a), Attenuation Factors for Certain Tissues when the Body is Exposed to Nearly Omni-directional Gamma Radiation, Brit. J. Radiol. 36,238

Spiers F W (1963b), Interim Report on the determination of dose to bone marrow from radiological procedures, Br. J. of Radiol. **36**, 424, 238-240

Spiers F W (1968), Radioisotopes in the Human Body, Academic Press

Spitzer V M and Whitlock D G (1998), Atlas of the visible human male, Jones and Bartlett, Boston, Mass., USA

Stabin M, Watson E, Cristy M, Ryman J, Eckerman K, Davis J, Marshall D and Gehlen K (1995), Mathematical models and specific absorbed fractions of photon energy in the nonpregnant adult female and at the end of each trimester of pregnancy, Report No. ORNL/TM-12907, Oak Ridge National Laboratory, Oak Ridge, Tenn., USA

Stabin M, Yoriyaz H (2002), Photon Specific Absorbed Fractions Calculated in the Trunk of an Adult Male Voxel-Based Phantom, Health Physics 82 (1)

Stuchly M (1996), In: The Zubal Phantom Data, Voxel-based Anthropomorphic Phantoms, http://noodle.med.yale.edu/phantom

Tanaka G, Nakahara Y and Nakajima Y (1989), Japanese Reference Man 1988-IV: studies on the weight and size of internal organs of normal Japanese, Nippon Igaku Hoshasen Gakkai Zasshi 49:344

Veit R, Zankl M, Petoussi N, Mannweiler E, Williams G. and Drexler G. (1989), Tomographic anthropomorphic models, Part I: Construction technique and description of models of an 8-week-old baby and a 7-year-old child, GSF-Report 3/89,GSF-National Research Center for Environment and Health, Neuherberg, Germany

Veit R, Panzer W, Zankl M and Scheurer C (1992), Vergleich berechneter und gemessener Dosen an einem anthropomorphen Phantom,Z.Med.Phys. 2:123-126

Vieira J W, Lima F R A and Kramer R (2002a), Bone dosimetry in the MAX – Male Adult voXel phantom for external exposures to photons in radiation protection. Paper presented at the International Topical Meeting on Industrial Radiation and Radioisotope Measurement Applications, 9-14 June 2002, Bologna, Italy.

Vieira J W, Lima F R A and Kramer R (2002b), Calculation of red bone marrow equivalent dose to the MAX (Male Adult voXel) model for external exposures to photons. Paper presented at the VI National Meeting on Nuclear Applications – ENAN,11.-16.8.2002, Rio de Janeiro, Brazil

Warner G G and Craig A M, ALGAM (1968), A Computer Program for Estimating Internal Dose for Gamma-Ray Sources in a Man Phantom, Oak Ridge National Laboratory, Oak Ridge, Tenn., USA, Report ORNL-TM-2250

Williams G, Zankl M, Abmayr W, Veit R and Drexler G (1986), The calculation of dose from external photon exposures using reference and realistic human phantoms and Monte Carlo methods, Phys. Med. Biol. 31:347-354

Xu X G, Chao T C, Bozkurt A (2000), VIP-MAN: An Image-based Whole-body Adult Male Model Constructed From Colour Photographs Of The Visible Human Project For Multi-particle Monte Carlo Calculations. Health Physics 78(5):476-486

Yoriyaz H, Santos A, Stabin M G, Cabezas R (2000), Absorbed fractions in a voxel-Based phantom calculated with the MCNP-4B code, Med Phys 27(7)1555-1562

Zankl M, Panzer W and Drexler G (1993), Tomographic Anthropomorphic Models. Part II: Organ Doses from Computed Tomographic Examinations in Paediatric Radiology.GSF-Bericht 30/93.Institut für Strahlenschutz, GSF-Forschungszentrum für Umwelt und Gesundheit, Neuherberg-Muenchen

Zankl M, Drexler G, Petoussi-Henss N, Saito K (1997), The Calculation of Dose from External Photon Exposures Using Reference Human Phantoms and Monte Carlo Methods. Part VII: Organ Doses due to Parallel and Environmental Exposure Geometries. GSF-Report 8/97. Institut fuer Strahlenschutz, GSF-Forschungszentrum fuer Umwelt und Gesundheit, Neuherberg-Muenchen

Zankl M, Panzer W and Herrmann C (2000), Calculation of Patient Doses Using a Human Voxel Phantom of Variable Diameter. Rad. Prot. Dos. Vol.90, Nos1-2, pp 155-158

Zankl M, Wittmann A (2001), The adult male voxel model "Golem" segmented from whole-body CT patient data. Radiat Environ Biophys 40: 153-162

Zankl M, Fill U, Petoussi-Henss N, Regulla D (2002a), Organ dose conversion coefficients for external photon irradiation of male and female voxel models, Phys Med Biol **47**, No.14, 2367-2386

Zankl M (2002b), Private communication, email from January 18

Zankl M, Petoussi-Henss N, Fill U and Regulla D (2002c), Tomographic anthropomorphic models. Part IV: Organ doses for adults due to idealized external photon exposures, GSF – National Research Center for Environment and Health, Neuherberg, Germany, GSF-Report (in preparation)

Zubal I G, Harrell C R, Smith E O, Rattner Z, Gindi G, Hoffer P B (1994a), Computerized three-dimensional segmented human anatomy. Med.Phys.21 No.2, 299-302

Zubal I G, Harrell C R, Smith E O, Smith A L and Krischlunas P (1994b), High resolution, MRI-based, segmented, computerized head phantom, In: The Zubal Phantom Data, Voxel-Based Anthropomorphic Phantoms,http://noodle.med.yale.edu/phantom

Zubal I G, Harrell C R, Smith E O and Smith A L (1995), Two dedicated software, voxel-based, anthropomorphic (torso and head) phantoms, In: Proceedings of an International Workshop on Voxel Phantom Development held at the National Radiological Protection Board,Chilton,UK,6-7 July

Zubal I G (2001), The Zubal Phantom Data, Voxel-Based Anthropomorphic Phantoms, http://noodle.med.yale.edu/phantom